NAVAL POSTGRADUATE SCHOOL

MONTEREY, CALIFORNIA

THESIS

VERIFICATION OF THE SINGLE SCATTERING ANALYTICAL MODEL FOR MODE COUPLING EFFECTS CAUSED BY SOLITONS

by

Jason Cornell

September 2009

Thesis Co-Advisors: John A. Colosi
Kevin B. Smith

Approved for public release; distribution is unlimited

REPORT DOCUMENTATION PAGE			Form Approved OMB No. 0704-0188
Public reporting burden for this collection of information is estimated to average 1 hour per response, including the time for reviewing instruction, searching existing data sources, gathering and maintaining the data needed, and completing and reviewing the collection of information. Send comments regarding this burden estimate or any other aspect of this collection of information, including suggestions for reducing this burden, to Washington headquarters Services, Directorate for Information Operations and Reports, 1215 Jefferson Davis Highway, Suite 1204, Arlington, VA 22202-4302, and to the Office of Management and Budget, Paperwork Reduction Project (0704-0188) Washington DC 20503.			
1. AGENCY USE ONLY ***(Leave blank)***	**2. REPORT DATE** September 2009	**3. REPORT TYPE AND DATES COVERED** Master's Thesis	
4. TITLE AND SUBTITLE Verification of the Single Scattering Analytical Model for Mode Coupling Effects Caused by Solitons		**5. FUNDING NUMBERS**	
6. AUTHOR(S) Jason E. Cornell			
7. PERFORMING ORGANIZATION NAME(S) AND ADDRESS(ES) Naval Postgraduate School Monterey, CA 93943-5000		**8. PERFORMING ORGANIZATION REPORT NUMBER**	
9. SPONSORING /MONITORING AGENCY NAME(S) AND ADDRESS(ES) N/A		**10. SPONSORING/MONITORING AGENCY REPORT NUMBER**	
11. SUPPLEMENTARY NOTES The views expressed in this thesis are those of the author and do not reflect the official policy or position of the Department of Defense or the U.S. Government.			
12a. DISTRIBUTION / AVAILABILITY STATEMENT Approved for public release; distribution is unlimited		**12b. DISTRIBUTION CODE**	

13. ABSTRACT (maximum 200 words)

The shallow-water environment poses many obstacles to submerged and surface operations. Not least of them are the obstacles posed to acoustic detection of quiet contacts. The presence of Internal Solitary Waves (ISWs) within this environmet induce acoustic variability and phase fluctuations, which limit signal processing capability and further complicate operations in this environment. However, a better understanding of how ISWs affect sound propagation may lead us to take advantage of some of the effects of the ISWs, such as how ISWs focus acoustic energy into certain modes allowing detection of quiet sources above background noise. An understanding of the phase fluctuation may also lead to better processing algorithms. While multiple numerical simulations have been conducted, which allow for the effects of ISWs to be intuited from them, an analytical model that can predict the effects on acoustic propagation by the physical parameters of the ISWs had not been produced until Professor John A. Colosi of the Naval Postgraduate School developed a single scattering analytical model of those effects.

In this thesis, the Colosi Single Scattering model will be compared to an accepted 3-D PE model in order to further validate the model. In the comparison, numerous simulations from both models have been used to determine how closely the Single Scattering model can predict the vertical mode coupling effects of ISWs.

14. SUBJECT TERMS Shallow-water environment, 3-D Simulations, Vertical Mode Coupling, Internal Solitary Waves, Solitons, Acoustic Variability			**15. NUMBER OF PAGES** 73
			16. PRICE CODE
17. SECURITY CLASSIFICATION OF REPORT Unclassified	**18. SECURITY CLASSIFICATION OF THIS PAGE** Unclassified	**19. SECURITY CLASSIFICATION OF ABSTRACT** Unclassified	**20. LIMITATION OF ABSTRACT** UU

NSN 7540-01-280-5500 Standard Form 298 (Rev. 2-89)
Prescribed by ANSI Std. 239-18

THIS PAGE INTENTIONALLY LEFT BLANK

Approved for public release; distribution is unlimited

VERIFICATION OF THE SINGLE SCATTERING ANALYTICAL MODEL FOR MODE COUPLING EFFECTS CAUSED BY SOLITONS

Jason E. Cornell
Lieutenant, United States Navy
B.S., West Virginia University Institute of Technology, 2002

Submitted in partial fulfillment of the
requirements for the degree of

MASTER OF SCIENCE IN APPLIED PHYSICS

from the

NAVAL POSTGRADUATE SCHOOL
September 2009

Author: Jason E. Cornell

Approved by: John A Colosi
Thesis Co-Advisor

Kevin B. Smith
Thesis Co-Advisor

James Luscombe
Chairman, Department of Physics

THIS PAGE INTENTIONALLY LEFT BLANK

ABSTRACT

The shallow-water environment poses many obstacles to submerged and surface operations. Not least of them are the obstacles posed to acoustic detection of quiet contacts. The presence of Internal Solitary Waves (ISWs) within this environmet induce acoustic variability and phase fluctuations, which limit signal processing capability and further complicate operations in this environment. However, a better understanding of how ISWs affect sound propagation may lead us to take advantage of some of the effects of the ISWs, such as how ISWs focus acoustic energy into certain modes allowing detection of quiet sources above background noise. An understanding of the phase fluctuation may also lead to better processing algorithms. While multiple numerical simulations have been conducted, which allow for the effects of ISWs to be intuited from them, an analytical model that can predict the effects on acoustic propagation by the physical parameters of the ISWs had not been produced until Professor John A. Colosi of the Naval Postgraduate School developed a single scattering analytical model of those effects.

In this thesis, the Colosi Single Scattering model will be compared to an accepted 3-D PE model in order to further validate the model. In the comparison, numerous simulations from both models have been used to determine how closely the Single Scattering model can predict the vertical mode coupling effects of ISWs.

THIS PAGE INTENTIONALLY LEFT BLANK

TABLE OF CONTENTS

LIST OF FIGURES

THIS PAGE INTENTIONALLY LEFT BLANK

LIST OF TABLES

THIS PAGE INTENTIONALLY LEFT BLANK

ACKNOWLEDGMENTS

I would like to thank Professor John Colosi for his guidance and the use of his model on which my entire thesis was based. I would also like to thank Professor Kevin Smith for the use of his PE model and his guidance in the use of the model. Both professors contributed to the editing and structuring of this thesis.

I. INTRODUCTION

Shallow-water Internal Solitary Waves (ISW) have been observed in a variety of locations including: the Massachusetts Bay, the New York Bight, Gulf of California, Andaman Sea offshore Thailand, the Australian North West Shelf, the Sulu Sea between the Philippines and Borneo, off the coast of Portugal, off Hainan Island in the South China Sea, and off the Strait of Gibraltar in the Alboran Sea (Zhou, Zhang, and Rogers, 1991). These shallow-water ISWs have soliton like characterizations such as: well-defined wavelengths, propagation in packets towards the shoreline, higher than linear group velocity, and decrease in wavelength and amplitude toward the rear of the packet (Zhou, Zhang, and Rogers, 1991). The solitons are caused by tidal driven flows over unusual bathymetry, such as sills and edges of continental shelves, and occur during the summer months when there is a strong thermocline near the surface and the layer is highly stratified (Zhou, Zhang, and Rogers, 1991). Figure 1 shows the effects of a soliton packet on the sound speed profile (ssp) within the water column. These perturbations to the ssp can cause unusually high transmission loss due to vertical mode coupling. This transmission loss has a resonance like behavior that is a function of acoustic source frequency and effective width of the soliton, where the effective width of the soliton refers to the distance traveled by the acoustic energy passing through each individual soliton (Zhou, Zhang, and Rogers, 1991; Colosi, 2008).

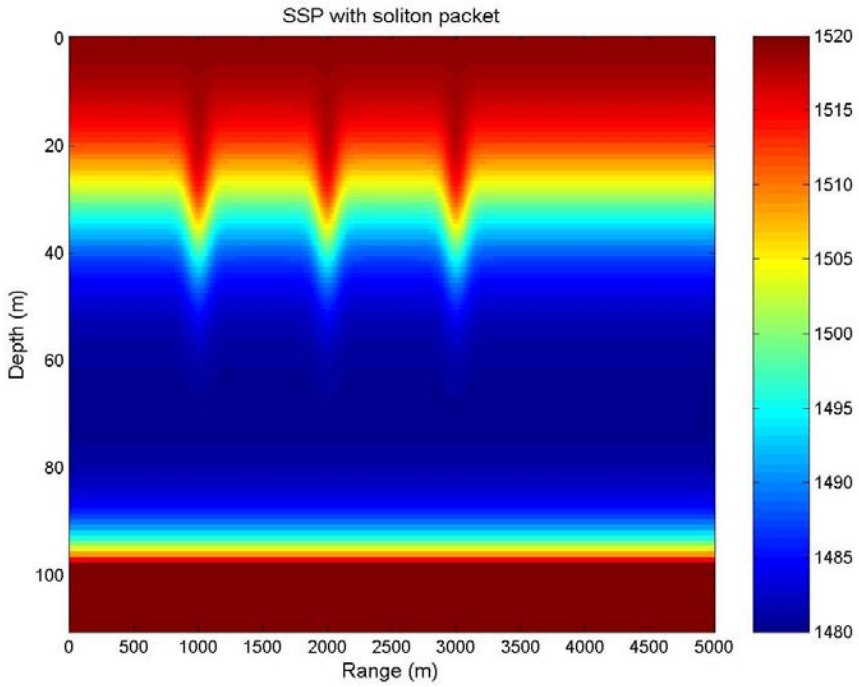

Figure 1. A Three Soliton Packet Supper Imposed on the SSP of a 100 m Deep Sound Channel

Prior to Professor John Colosi of the Naval Postgraduate School developing the Single Scattering Analytical Model for 2-D acoustic mode propagation through a soliton, there were no analytical descriptions of what effects solitons have on vertical mode coupling (Colosi, 2008). An analytical model, which can mathematically model the effects of solitons on mode coupling, is beneficial to improving processing algorithms. This paper seeks to validate the Single Scattering Analytical Model by direct comparison of its results with a 3-D Parabolic Equation Model. A Parabolic Equation model is used as a benchmark in this analysis, since this type of model has been proven to produce results consistent with real world experiments (Smith, 2001). The results will be compared for propagation through both a single soliton and a soliton packet for multiple orientations of the solitons. The comparison will be based on the ratio of modal energies (RME). The RME is a measure of energy coupled into or out of a particular mode. The resonance behavior exhibited by the mode coupling is compared as well by predicting the resonance location of the PE model using the analytical model.

II. HOW THE PE MODEL WORKS

A. INTRODUCTION

In this chapter, a brief description of the 3-D implementation of the Monterey Miami Parabolic Equation (3DMMPE) model is given (Smith and Colosi, 2008). The description shall cover the pertinent material from the SWAM99 article Professor Smith published in the Journal of Computational Acoustics (JCA) (Smith, 2001), and the extension to 3-D. The first part of the discussion covers how the parabolic equation was developed. Next, a discussion of the split-step Fourier algorithm is given. Lastly, the method for modal decomposition is explained.

B. DEVELOPMENT OF THE PARABOLIC EQUATION

In this section, the development of the 3DMMPE is discussed, as well as aspects that are unique to this particular PE model. This section closely follows the SWAMM99 article for the development of the PE (Smith, 2001). This reference is presented to prevent excessive duplicate references in the following section. Unlike the SWAMM99 article, the PE is developed in terms of Cartesian coordinates instead of cylindrical coordinates.

First, the time-harmonic acoustic field is defined in Cartesian coordinates as

$$P(x,y,z,t) = p(x,y,z)e^{i\omega t}. \tag{1}$$

Substitution into the wave equation results in the Helmholtz equation,

$$\nabla^2 p(x,y,z) + k_o^2 n^2(x,y,z)\, p(x,y,z) = -4\pi P_o \delta(z - z_s). \tag{2}$$

The k_o value is the reference sound speed and is defined as $k_o = \omega / c_o$, and n is the index of refraction defined as $n = c_o / c(x,y,z)$. The c_o value is the reference acoustic sound speed, which is picked so that all values of n^2 are near unity. The acoustic sound speed $c(x,y,z)$ contains all of the features of the environment including the sound speed perturbation caused by the solitons. The term on the right hand side of equation is the source term which approximates the source located at $x = 0$, $y = 0$, and $z = z_s$. Setting the

right hand side to zero allows the homogenous Helmholtz equation to be solved for the acoustic pressure. Rewriting the Helmholtz equation in terms of the partial derivatives yields

$$\frac{\partial^2 p}{\partial x^2}+\frac{\partial^2 p}{\partial y^2}+\frac{\partial^2 p}{\partial z^2}+k_o^2 n^2 p=0\,. \tag{3}$$

Introducing the operators

$$P_{op}=\frac{\partial}{\partial x},\quad u=\frac{1}{k_o^2}\frac{\partial^2}{\partial z^2},\quad v=\frac{1}{k_o^2}\frac{\partial^2}{\partial y^2},\ \text{ and }\ \varepsilon=n^2-1 \tag{4}$$

allows the Helmholtz to be rewritten as

$$\left\{P_{op}^2+k_o^2\left[v+u+\varepsilon+1\right]\right\}p=0\,. \tag{5}$$

Introducing the operator $Q_{op}=(u+v+\varepsilon+1)^{1/2}$ further simplifies the Helmholtz equation to

$$\left\{P_{op}^2+k_o^2 Q_{op}^2\right\}p=0\,. \tag{6}$$

Equation 6 can be factored to

$$\left(P_{op}+ik^2 Q_{op}\right)\left(P_{op}-ik^2 Q_{op}\right)p+ik_o\left[P_{op},Q_{op}\right]p=0\,, \tag{7}$$

where it represents the factorization of the field into incoming and outgoing waves (Smith, 2001; Smith, 2005). If the commutator ($[P_{op},Q_{op}]$) is taken to be zero for layered media, and the substitution $p=Q_{op}^{-1/2}\Psi$ is made, the outgoing wave then satisfies

$$P_{op}\Psi=ik_o Q_{op}\Psi\,. \tag{8}$$

Defining Ψ in terms of the PE field function ψ such that $\Psi=\psi e^{ik_o x}$, then the outgoing field function (Equation 8) can be written in terms of the evolution of the PE field function in the x-direction, i.e.,

$$\frac{\partial\psi}{\partial x}=ik_o(Q_{op}-1)\psi=-ik_o H_{op}\psi \tag{9}$$

The acoustic pressure field can then be determined from the PE field function by

$$p(x,y,z)=P_o\sqrt{\frac{R_o}{r}}Q_{op}^{-1/2}\psi(x,y,z)e^{ik_o x}\,. \tag{10}$$

Here, P_o refers to the source acoustic pressure at a reference range R_o, and r is the horizontal slant range $r = \sqrt{x^2 + y^2}$

C. DESCRIPTION OF THE SPLIT-STEP FOURIER ALGORITHM

Now that an expression for the evolution of the PE field function in range (x-direction) has been developed in Equation 9, all that is needed is an algorithm to solve for ψ. Equation 9 can be rewritten in the form

$$\psi(r + \Delta r) = \Phi(r)\psi(r), \tag{11}$$

where $\Phi(r)$ represents the propagator of $\psi(r)$. For small range steps Δr, the propagator can be approximated by (Smith, 2005)

$$\Phi(r) = e^{-ik_o \Delta r \bar{H}_{op}(r)}. \tag{12}$$

To implement the SSF algorithm the H_{op}, and therefore the Q_{op}, must be separable. Specifically, the u and v operators need to be separated from the ε operator. In the 3DMMPE, this is accomplished with the Thompson and Chapman (Smith, 2005) approximation for the Q_{op}. This approximation allows the Q_{op} to be represented by

$$Q_{op} = \sqrt{1 + u + v + \varepsilon} \approx \sqrt{1 + u + v} + \sqrt{1 + \varepsilon} - 1 = 1 - T_{op} - U_{op}, \tag{13}$$

where

$$T_{op} = 1 - \sqrt{1 - u + v} \quad \text{and} \quad U_{op} = 1 - \sqrt{1 + \varepsilon}. \tag{14}$$

Recall from Equation 9 that $H_{op} = 1 - Q_{op}$, which when substituted into Equation 12 yields

$$\Phi(r) = e^{-ik_o \Delta r (Q_{op} - 1)} = e^{ik_o \Delta r (T_{op} + U_{op})}. \tag{15}$$

Using the Baker-Campbell-Hausdorff expansion (Bellman, 1964), Equation 15 can be rewritten

$$\Phi(r) = e^{ik_o \Delta r (T_{op} + U_{op})} = e^{ik_o \frac{\Delta r}{2} U_{op}(r + \Delta r)} e^{ik_o \Delta r T_{op} \left(\frac{\partial^2}{\partial z^2} + \frac{\partial^2}{\partial y^2} \right)} e^{ik_o \frac{\Delta r}{2} U_{op}(r)}. \tag{16}$$

Substituting Equation 16 back into Equation 11 yields

$$\psi(r + \Delta r) = e^{ik_o \frac{\Delta r}{2} U_{op}(r + \Delta r)} e^{ik_o \Delta r T_{op} \left(\frac{\partial^2}{\partial z^2} \right)} e^{ik_o \frac{\Delta r}{2} U_{op}(r)} \psi(r). \tag{17}$$

The U_{op} is a scalar in z-space and, therefore, is a diagonal matrix that can be multiplied with $\psi(r)$. The T_{op} is a differential operator in terms of z and y, so that different depth eigenfunctions are coupled. As a result, the T_{op} is not a diagonal operator in z-space and cannot just be multiplied with the $\psi(r)$ term. The operation of T_{op} on $\psi(r)$ in (y,z)-space would then be a time and memory intensive process. An alternative approach would be to take the Fourier Transform of $\psi(r)$ and then operate on it in (k_y, k_z)-space. The benefit of performing the operation in (k_y, k_z)-space is that $\hat{T}_{op}$ is a diagonal matrix and, therefore, is a scalar multiplication operation with $\hat{\psi}(r)$. Here, $\hat{T}_{op}$ is equal to

$$\hat{T}_{op} = 1 - \sqrt{1 - \left[\frac{k_z^2 + k_y^2}{k_o^2} \right]}. \tag{18}$$

The inverse Fourier Transform of $\hat{\psi}(r)$ can then be taken before performing the scalar multiplication operation with U_{op}. This is exactly the approach taken in the Split-Step Fourier Algorithm, shown symbolically below.

$$\psi(x + \Delta x, y, z) = e^{-ik_o \frac{\Delta x}{2} U_{op}(x + \Delta x)} IFFT \left\{ e^{-ik_o \Delta x \hat{T}_{op}(k_z, k_y)} * FFT \left[e^{-ik_o \frac{\Delta x}{2} U_{op}(x)} \psi(x, y, z) \right] \right\} \tag{19}$$

D. METHOD FOR MODAL DECOMPOSITION

In this section, the method used to extract the modal amplitudes (A_n) from the acoustic pressure field computed by the PE model is discussed. This discussion includes why the normal mode shape can be used as the basis set for the wave equation. Errors introduced by the Thompson Chapman approximation will also briefly be discussed.

Smith used a separation of variables technique to obtain the depth separable wave equation (Smith, 2005). First, the acoustic pressure is defined by

$$p(x, y, z) = \Phi(x, y)\Psi(z), \tag{20}$$

where $\Phi(x,y)$ is a range dependent Bessel function, and $\Psi(z)$ is the normal mode of the waveguide. Substitution into Equation 3 yields

$$\Psi\frac{\partial^2\Phi}{\partial x^2}+\Psi\frac{\partial^2\Phi}{\partial y^2}+\Phi\frac{\partial^2\Psi}{\partial z^2}+k_o^2n^2\Phi\Psi=0\,. \tag{21}$$

Separation of the x, y, and z dependent terms yields

$$\frac{1}{\Phi}\frac{\partial^2\Phi}{\partial x^2}+\frac{1}{\Phi}\frac{\partial^2\Phi}{\partial y^2}+\frac{1}{\Psi}\frac{\partial^2\Psi}{\partial z^2}+k_o^2n^2=0\,. \tag{22}$$

The first and second term of Equation 22 depends on x and y, while the third term depends only on z. Therefore, for the equation to sum to zero the first two terms and the last two terms on the left side must sum to equal the same constant but of different sign. Smith used the square of the horizontal wavenumber (K) as the separation variable (Smith, 2005), which yields the depth separated wave equation

$$\frac{\partial^2\Psi}{\partial z^2}+k_o^2n^2\Psi=K^2\Psi\,. \tag{23}$$

It is well known that when boundaries are introduced in layered media, the propagation is characterized by the quantized modes defined by K_m (Smith, 2005), which yields

$$\frac{\partial^2\Psi_m}{\partial z^2}+k_o^2n^2\Psi_m=K_m^2\Psi_m\,. \tag{24}$$

Moving the right side of the equation to the left side yields and factoring out a k_o^2 term yields

$$\frac{\partial^2\Psi_m}{\partial z^2}+k_o^2(n^2-1)\Psi_m+k_o^2\left(1-\frac{K_m^2}{k_o^2}\right)\Psi_m=0\,. \tag{25}$$

Applying operators from Equation 4 yields

$$u\Psi_m+\varepsilon\Psi_m+\left(1-\frac{K_m^2}{k_o^2}\right)\Psi_m=0\,, \tag{26}$$

where we can introduce the operator q defined by $q = u + \varepsilon$. Substituting this operator into Equation 26 yields

$$q\Psi_m = \left(\frac{K_m^2}{k_o^2} - 1 \right) \Psi_m . \tag{27}$$

From Equation 27, we can deduce that a wave equation based on the q operator has the normal mode shapes as its basis set (Smith, 2005). It can also easily be shown that these modes are identical to the standard normal modes of the Helmholtz equation (Smith and Smith, 1998).

Therefore, for such wave equations we can assume the acoustic pressure field can be expressed as

$$p(x,y,z) = \sum_{n=1}^{N} A_m(x,y)\Psi_m(z) . \tag{28}$$

The modal amplitudes are then equal to (Smith, 2005)

$$A_m = \int_0^\infty \frac{1}{\rho(z)} p(x,y,z)\Psi_m(z)\,dz . \tag{29}$$

The only issue left is our wave equation, as defined in Section B, based on the q operator. From Equation 13, the Q_{op} is defined as

$$Q_{op} = \sqrt{1 + u + v + \varepsilon} . \tag{30}$$

In a purely layered waveguide, the v operator can be neglected yielding

$$Q_{op} = \sqrt{1 + u + \varepsilon} , \tag{31}$$

which would be consistent with the q operator. However, since the PE uses the Thompson and Chapman approximation the Q_{op} is defined as

$$Q_{op} \approx \sqrt{1 + u} + \sqrt{1 + \varepsilon} - 1. \tag{32}$$

Therefore, the PE does not use the q operator exactly. According to Smith and Smith (1998), this introduces second order errors but can be minimized with the choice of value

for the reference sound speed (c_o). The result is that some modal amplitudes may exhibit fluctuations with range. Tests on the stability of the modal decomposition were performed in order to minimize the impact of this effect on the results presented in this thesis.

THIS PAGE INTENTIONALLY LEFT BLANK

III. HOW THE ANALYTICAL MODEL WORKS

A. INTRODUCTION

In this chapter, a brief description of the Single Scattering Analytical model is given. The description shall cover the pertinent material from an article Professor Colosi published in the Journal of the Acoustical Society of America (JASA) (Colosi, 2008) and from Chapter 6 of Introduction to Acoustic Fluctuation (Colosi and Flatte, 2008). The first part of the discussion covers how the expression for mode coupling was developed and how the expression was altered to account for multiple solitons. Lastly, an explanation is given for how the expression was utilized in the model.

B. AN EXPLANATION OF HOW THE ANALYTICAL EXPRESSION WAS DEVELOPED FOR MODE COUPLING INTO AND OUT OF A MODE

In this section, an explanation is given of how the analytical expression for mode coupling was developed. The explanation will follow closely the Colosi JASA article previously referenced (Colosi, 2008). This reference to the article is given now to prevent excessive references back to the article in this section. The explanation is reproduced again in this paper instead of just referencing the JASA article since excerpts will be taken from other sources in order to provide a sufficient explanation of the theory used in this analysis.

Colosi used the Creamer formalism for two-dimensional mode coupling in shallow-water to produce an expression for the change in modal energy due to acoustic propagation through a soliton (Creamer, 1996). The ssp was defined in range (r) and depth (z) by

$$c(r,z) = \overline{c}(z) + \delta c(r,z). \tag{33}$$

Here, $\overline{c}(z)$ is the background ssp and $\delta c(r,z)$ is the perturbation to the ssp caused by a soliton. The acoustic pressure field is defined in terms of the summation of the product of the modal amplitudes ($A_n(r)$) and the unperturbed vertical mode shapes ($\phi_n(z)$).

$$p(r,z) = \sum_{n=1}^{N} \frac{A_n(r)}{\sqrt{k_n r}} \phi_n(z). \tag{34}$$

Here, k_n is the modal wave number. The consequence of using the unperturbed vertical mode shape is that all of the acoustic variability is confined to the modal amplitude function. This fact will be exploited in Chapter IV of this paper by allowing for a comparison of the analytical and PE models by only comparing the change in modal energies, which are directly derived from the modal amplitudes. Colosi uses the quasistatic, narrow angle, weak forward scattering approximation of Dozier and Tappert (1978a), and Dozier (1983) to show that the scaled mode amplitude $\psi_n = A_n \exp(-il_n r)$ obeys the one-way equation

$$\frac{\partial \psi_n}{\partial r} = -i\sum_{m=1}^{N} \rho_{mn}(r) e^{il_{mn}r} \psi_m(r) \tag{35}$$

where $l_{mn} = l_m - l_n$ is the difference between complex horizontal wave numbers. Note that in this context, *n* is used to denote the mode of interest and *m* is used to denote the mode to which n is being coupled to. The symmetric coupling matrix ρ_{mn} is defined as

$$\rho_{mn}(r) = k_o \int_0^\infty u(r,z) \frac{\phi_n \phi_m}{\sigma(z)} dz\,. \tag{36}$$

Here, $\sigma(z)$ is the density profile as a function of depth, $u(r,z) = \delta c(r,z)/c_o$ is the fractional sound speed variance, k_o is the reference wave number, and c_o is the reference sound speed (Colosi and Flatte, 2008).

The change in ssp with depth is typically small in the natural environment. Therefore, the fractional sound speed variance caused by a soliton, which is a displacement of the layer in depth, is also typically small. Colosi used this fact to produce a solution to Equation 35 in terms of the Dyson Series (Dyson, 1949; Sakurai, 1985). The solution to second order is

$$\psi_n(R) = \psi_n(0) - i\sum_{m=1}^{N} \psi_m(0) S_{mn}^{(1)} - \sum_{m=1}^{N}\sum_{j=1}^{N} \psi_j(0) S_{mnj}^{(2)}\,, \tag{37}$$

where *R* corresponds to the receiver range. The first and second order scattering matrices $S_{mn}^{(1)}$ and $S_{mnj}^{(2)}$ are defined by

$$S_{mn}^{(1)} = \int dk \hat{\rho}_{mn}(k) \int_{-R/2}^{R/2} dr' e^{i(l_{mn}-k)r'} \tag{38}$$

and

$$S_{mnj}^{(2)} = \int dk \int dk' \hat{\rho}_{mn}(k) * \hat{\rho}_{jm}(k') \int_{-R/2}^{R/2} dr' \int_{-R/2}^{r'} dr'' e^{i((l_{mn}-k)r' + (l_{jm}-k')r'')} . \tag{39}$$

For the single scattering model, Colosi concluded that the second order scattering term in Equation 39 is typically small for the shallow-water conditions under consideration and therefore could be neglected without introducing a gross inaccuracy.

To further develop the expression for the mode coupling matrix ($\hat{\rho}_{mn}(k)$), Colosi defined the fractional sound speed variance in term of sound speed gradient (dc/dz), the vertical displacement of the soliton (ζ_o), the mode one vertical mode shape ($W_1(z)$), the parameter $F(r,t)$ which contains the variation in range and time caused by the soliton.

$$u(r,z,t) = \frac{-1}{c_o}\left(\frac{dc}{dz}(z)\right)\zeta_o W_1(z) F(r,t) \tag{40}$$

.

Substituting Equation 40 into Equation 36 then yields

$$\rho_{mn}(r,t) = k_o \int_0^\infty \frac{-1}{c_o}\left(\frac{dc}{dz}(z)\right)\zeta_o W_1(z) F(r,t) \frac{\phi_n(z)\phi_m(z)}{\sigma(z)} dz . \tag{41}$$

If the contribution to mode coupling from the depth dependence of the soliton and the mode structure is defined as

$$Z_{mn} = \frac{-\zeta_o k_o}{c_o} \int_0^\infty \left(\frac{dc}{dz}(z)\right) W_1(z) \frac{\phi_n(z)\phi_m(z)}{\sigma(z)} dz , \tag{42}$$

then the mode coupling matrix is defined as

$$\rho_{mn}(r,t) = F(r,t) Z_{mn} . \tag{43}$$

Colosi uses a Gaussian function to represent the range and time dependence associated with a soliton, where

$$F(r,t) = \exp\left[\frac{-(r - r_o(t))^2}{\Delta^2}\right]. \tag{44}$$

Here, $r_o(t)$ and Δ are the position and width of the soliton, respectfully. Substitution of Equations 42, 43, and 44 back into Equation 38 and integrating yields

$$S_{mn}^{(1)} = \sqrt{\pi} Z_{mn} \Delta \exp\left[\frac{-k_{mn}^2 \Delta^2}{4}\right] e^{ik_{mn} r_o} \quad . \tag{45}$$

An expression for the modal energies can now be defined in terms of the physical parameters of the soliton. The modal energies will be defined as the square of the magnitude of the modal amplitudes. First, $A_n(r)$ will be substituted for $\psi_n(r)$ in Equation 37, and then multiplied by its complex conjugate. After dropping the second order terms for the single scattering approximation the result is

$$\left|A_n(R)\right|^2 = \left|A_n(0)\right|^2 + 2\sum_{m=1}^{N} A_n(0) A_m(0) \operatorname{Im}\left(S_{mn}^{(1)}\right). \tag{46}$$

Substitution of Equations 45 into Equation 46 then yields

$$\left|A_n(R)\right|^2 = \left|A_n(0)\right|^2 + 2\sqrt{\pi}\sum_{n=1}^{N} A_n(0) A_m(0) Z_{mn} \Delta_f \exp\left[\frac{-k_{mn}^2 \Delta_f^2}{4}\right] \sin(k_{mn} r_o). \tag{47}$$

This is the expression used in the model to determine the change in modal energy after acoustic propagation through a soliton.

There are three fundamental assumptions made in the development of this theoretical model that are worth re-stating here as they may impact the subsequent comparisons between the theoretical predictions and the solutions computed from the 3DMMPE model. These assumptions are:

1) the interactions of the field with the ISW perturbation are only 2-dimensional;
2) the coupling introduced by the forward scattering is assumed to be relatively weak; and
3) only first order coupling effects are considered.

While the second assumption may be considered a reasonable approximation of the interactions of the field with the ISW, the impact of the first and third assumptions are unknown. Potential effects observed in the analysis will be discussed later.

1. Explanation of How the Analytical Expression Is Altered to Account for Propagation through Multiple Solitons

In this section, the terms are identified that account for multiple solitons. How these terms are altered and what changes in the code are required to apply the alterations. The variables that can change based on the number of solitons are ζ_o, Δ, and r. All of these variables can be accounted in our expression for the modal energies by adding a summation to Equation 45 yielding

$$S_{mn}^{(1)} = \sqrt{\pi} \sum_{p=1}^{N_s} Z_{mn}(p) \Delta_p \exp\left[\frac{-k_{mn}^2 \Delta_p^2}{4} \right] e^{ik_{mn} r_o(p)} . \tag{48}$$

Equation 42 changed by allowing the vertical displacement of the soliton to change from one soliton to another yielding

$$Z_{mn} = \frac{-\zeta_o(p) k_o}{c_o} \int_0^\infty \left(\frac{dc}{dz}(z) \right) W_1(z) \frac{\phi_n(z) \phi_m(z)}{\sigma(z)} dz . \tag{49}$$

As shown in Figure 2, all of the mode coupling effects from the solitons are applied at the axis of the first soliton in the packet. For this reason, a line was superimposed on the RME field to identify where the end of the packet is located. As a result of where the mode coupling effects are applied, the RME field is not valid for the analytical model until after the soliton packet. In the analysis presented in this paper, comparisons between the models are only made for the RME field after the packet.

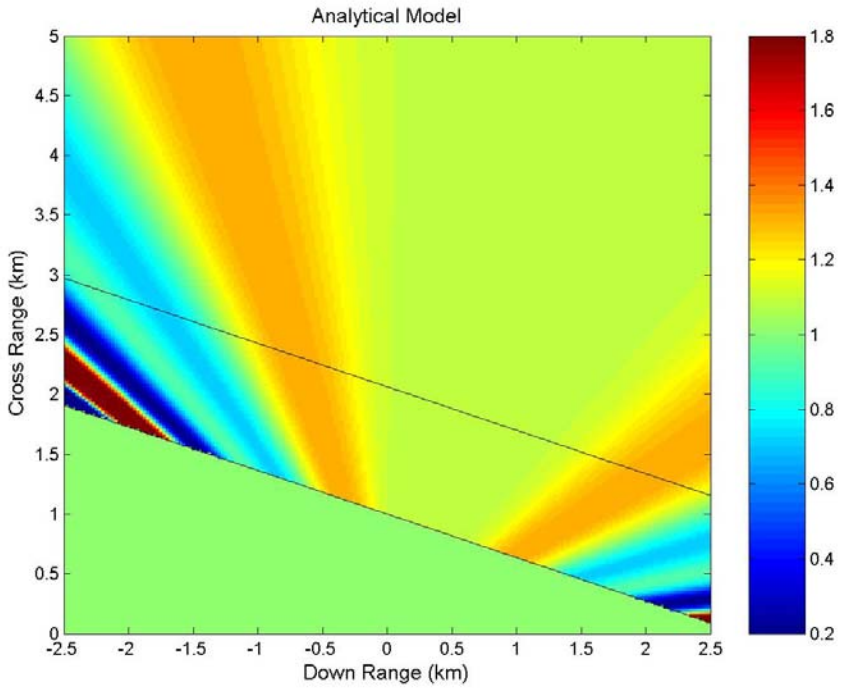

Figure 2. Ratio of Modal Energies (mode 1, 150 Hz, 20^{o} soliton angle)

C. EXPLANATION OF HOW THE ANALYTICAL EXPRESSION FOR MODE COUPLING IS UTILIZED IN THE MODEL

In this section, the procedure used by the analytic model to implement Equation 47 is briefly explained. An explanation of how the model deals with changing effective soliton widths is also given. A sample of the results is also explained using Equation 47.

Figure 3 is an example of a surface plot of the RMEs. First, the model breaks up the 2-D field into angles of propagation from the source. Here, the 2-D field corresponds to the 2-D surface plot that the RME field will be superimposed onto. Then, the distance from the source to the soliton (r_o) is calculated for each angle of propagation. The r_o values are stored in a vector that references the distance to the angle of propagation. The model then inserts the physical parameters of the soliton and the r_o values into Equation 47 and the corresponding value of modal energy is stored in an NxM matrix referenced to the angle of propagation and the mode number. Each modal energy value is divided by the initial modal energy value at the source. The resultant value is the RME of the

perturbed and unperturbed field. The RME is then a normalized value, which gives the amount of energy coupled into or out of the particular mode.

Note that the soliton width in Equation 47 corresponds to the effective soliton width (Δ_f). Due to the spherical propagation the acoustic path will incident onto the soliton at different angles. Therefore, when the soliton is oriented horizontally, the distance traveled by the acoustic energy in order to cross the soliton increases with increasing angle of propagation from the zero cross-range axis. The model accounts for the change in the effective width by $\Delta_f = \Delta / \cos\theta$, where Δ is the actual width of the soliton and θ is the angle measure between the acoustic path and the vertical axis.

The RME field is divided up into an NxM grid with each grid segment corresponding to a cell within an NxM matrix. The distance from the source to each cell r_o is calculated along with angle of propagation from the source. If $r \geq r_o$, then the cell is assigned the RME value corresponding to its angle of propagation. If $r < r_o$ then the cell is assigned the value of one. The NxM matrix is then plotted onto a surface plot against the down range and cross range values from the source as in Figure 3.

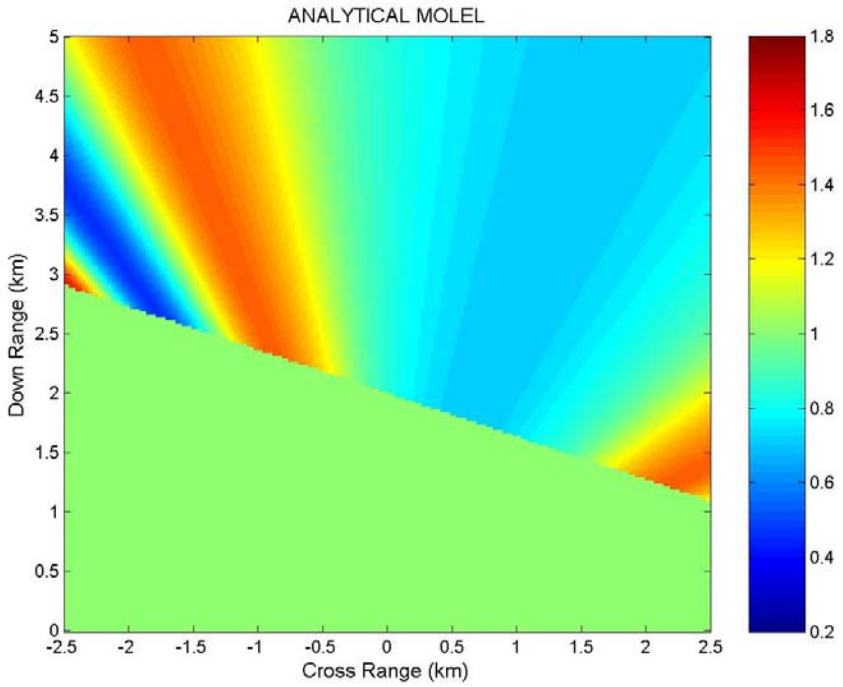

Figure 3. Ratio of Modal Energies (mode 1, 150 Hz, 20^o soliton angle)

The features in Figure 3 can be explained through the use of Equation 47. As r_o increases along the length of the soliton with respect to k_{mn}, the second term in the expression oscillates sinusoidally with the sine function. This explains the striation pattern after the soliton. Also, as Δ_f increases along the length of the soliton, it causes competing effects in the second term of Equation 47. For the range over which Δ_f changes the dominant effect is to increase the magnitude of the second term. Therefore, the magnitude of the ratios will increase with increasing Δ_f along the length of the soliton.

IV. VALIDATION OF ANALYTICAL MODEL WITH 3DMMPE MODEL

A. COMPARISON OF THE ANALYTICAL MODEL WITH THE PE NUMERICAL MODEL FOR VARYING ORIENTATIONS OF THE SOLITON

In this section, the results of the PE numerical model and the analytical model will be compared for the purpose of validating the predictions of the theory. The comparison will be based on the correlation of the RMEs. This approach is valid since both techniques assume that the acoustic variability introduced by the mode coupling effects is confined to the modal amplitudes. The RME is then defined by

$$RME = \frac{|A_n(r)|^2_{perturbed}}{|A_n(r)|^2_{unperturbed}}. \tag{50}$$

In this notation, the unperturbed modal energy refers to the acoustic field without a soliton present and perturbed refers to the acoustic field with a NLIW present.

Two criteria will be used to measure how well the RMEs correlate. The first will be a normalized correlation coefficient, which is a measure of how well the different regions of mode coupling align geometrically (Rodgers and Nicewander, 1988). The second will be a comparison of the magnitude of the RMEs.

1. Comparison of the PE Numerical Model with the Analytical Model for a Single Soliton Perpendicular to the Main Direction of Acoustic Propagation

In this section, the models will be compared for the case where propagation of the soliton is in the same direction as the *x*-axis. This orientation will be referred to as the 0^o soliton angle, where the soliton angle is the angle between the propagation of the soliton and the central radial acoustic propagation. In this case, the central radial of the acoustic energy will be incident at a normal angle to the soliton, where the mode coupling occurs entirely in the vertical plane (Colosi, 2008). First, a surface plot of the RME from each model will be compared qualitatively for geometric orientation and magnitude. Then, a

line plot of the RMEs at 5 km from the source will be used in order to make a quantitative comparison of the geometric orientation and magnitude.

Figure 4 is the RME distribution for mode 1 at 150 Hz produced by the PE model. Figure 5 is the similar RME distribution as computed by the analytical model. Both plots show a striation pattern in the RME field after the soliton. The size and general orientation of the striation patterns are comparable. Specifically, the striation patterns are symmetric about the center of the plot with roughly the same magnitude of RME. However, the analytical model shows an extra defocusing region starting at 2 km cross range just after the soliton. This suggests that the width of the striation patterns for the PE is slightly wider than predicted by the analytical model. The deviation from unity of the RME for the analytical model is also consistently larger than for the PE. This could be the result of the model implementing the initial conditions differently. More than likely, it is a second order scattering effect which as discussed in Chapter III, this analytical model does not account for. The PE results in Figure 4 also contain an oscillation in the striation pattern that oscillates as a function of range for a fixed angle of propagation. This oscillation is not present in the analytical predictions. This is likely due to very minor 3-D horizontal refraction effects, which are not accounted for in the 2-D assumption of the theory. The comparison of the surface plots for the other three modes analyzed (two, four, and five) had similar qualitative results.

It is important to note that Figures 4 and 5 are the ratio of the modal energies (RME) for the perturbed and unperturbed acoustic fields $\left(\left| A_n(r) \right|^2_{pert} \Big/ \left| A_n(r) \right|^2_{unpert} \right)$. Therefore, this is a comparison of the amount of mode coupling that occurs in each model, not a direct comparison of the modal amplitude distribution of each model. Also, the striation pattern present in each figure is made up of focusing and defocusing regions as a result of vertical mode coupling caused by propagation through the soliton. The physical consequence of the sinusoidal fluctuation is that the RME field is made up of regions where modal energy is transferred to or from one mode to another. Modal energy is transferred to the mode in the focusing regions and out of the mode in the defocusing region.

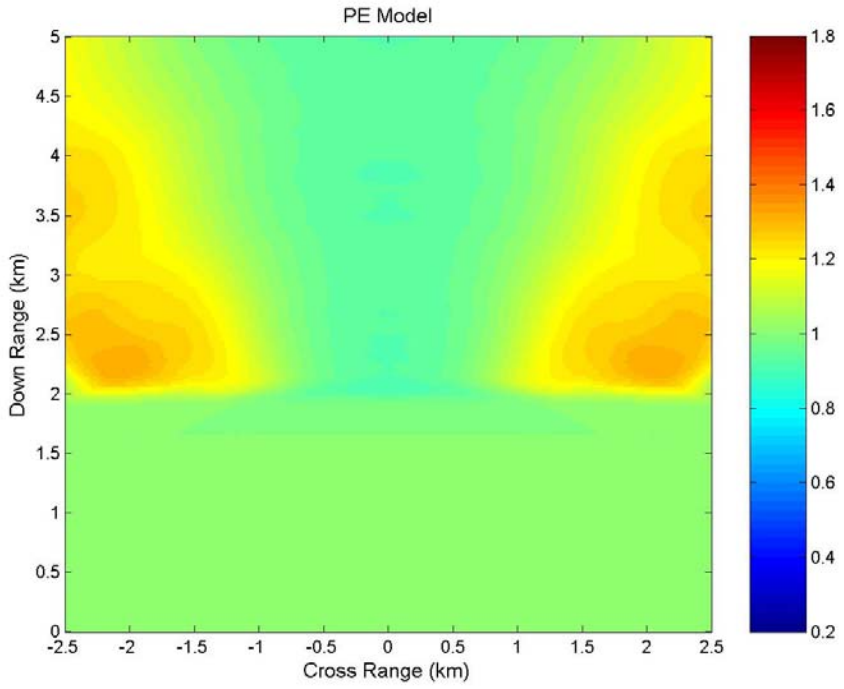

Figure 4. Ratio of Modal Energies (mode 1, 150 Hz, 0^o soliton angle)

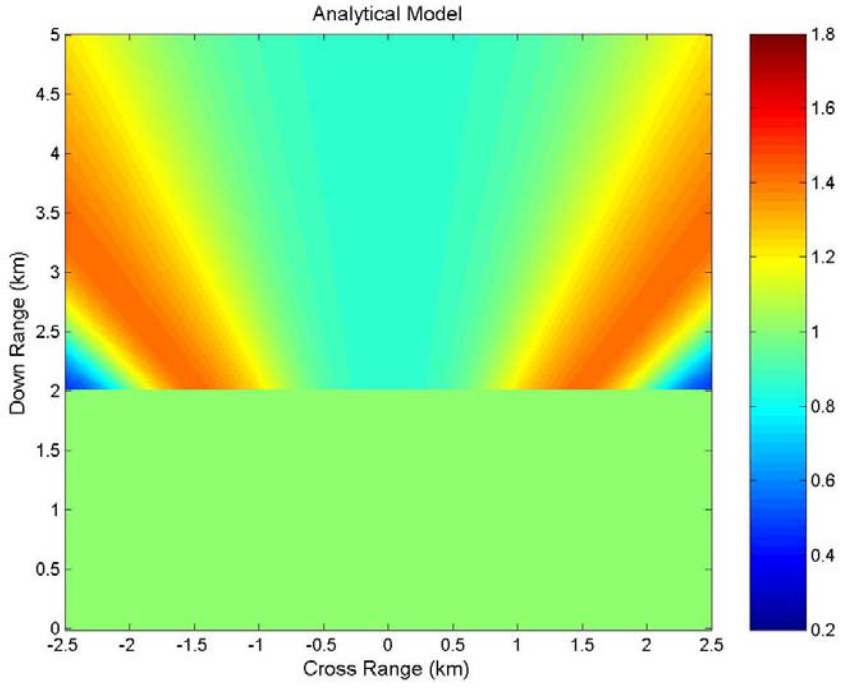

Figure 5. Ratio of Modal Energies (mode 1, 150 Hz, 0^o soliton angle)

Some explanation should be given for the oscillation in the focusing pattern shown in Figure 4, and why it does not show up in Figure 5. For the Single Scattering Approximation used in the analytical model, all of the mode coupling effects of the soliton is accounted for at the center of the soliton located at 2 km down range in Figure 4. Therefore, the analytical model would not account for coupling effects down range of the soliton without accounting for second order or higher scattering effects (Colosi, 2008). The fluctuations in Figure 4 for the PE model are possibly a numerical artifact, since they occur in regions where the ssp is not a function of range from the source. However, such fluctuations are not present at higher soliton angles (see, for example, Figure 11) and suggest that this feature has a physical manifestation. It could be a 3-D, horizontal refraction effect which the 2-D model would not compute. The PE model was not run in an Nx2-D implementation to confirm this, unfortunately. Future work will attempt to address this effect, both numerically and theoretically. The effect is not significant for modes 1 and 2, however, in modes 4 and 5 the oscillations are closer together and change the look of the field considerably. Figures 6 and 7 are the surface plots for mode 5 produced by the PE model and analytical model.

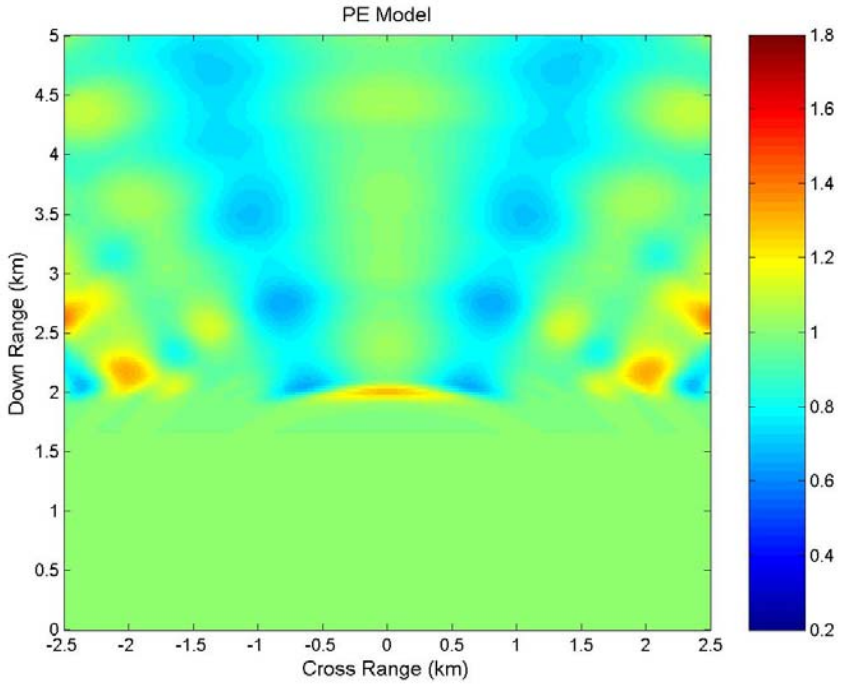

Figure 6. Ratio of Modal Energies (mode 5, 150 Hz, 0^o soliton angle).

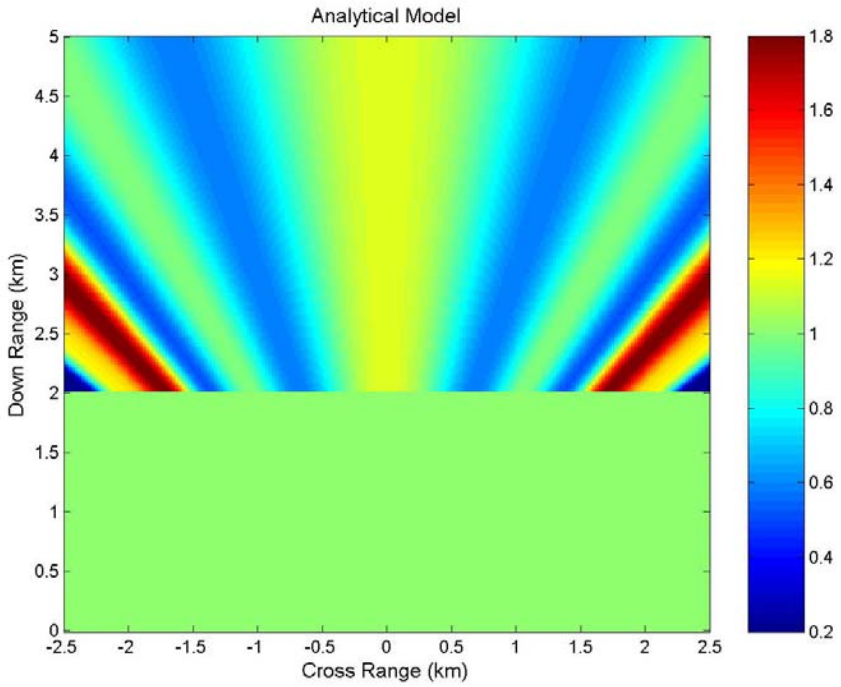

Figure 7. Ratio of Modal Energies (mode 5, 150 Hz,0^{o} soliton angle).

A quantitative comparison of the correlations can be made by looking only at the RME for both predictions at a specific range. Figure 8 is a line plot of the RMEs at 5 km down range, with the PE ratio in blue and the analytical ratio in red. The range for the comparison was chosen to be at 5 km to stay consistent with other line comparisons presented later in this paper. A range of 3 km may have been a better choice for comparing the results for this soliton angle. However, the results did not change appreciably when analyzed at 3 km.

As noted from the surface plots, Figure 8 shows that the predicted amount of mode coupling is consistently greater for the analytical model. The largest difference in the magnitude of mode coupling occurred at 0 km cross range and resulted in 8% more mode coupling in the analytical model. The regions of mode coupling geometrically align very well with a correlation coefficient of 0.9997.

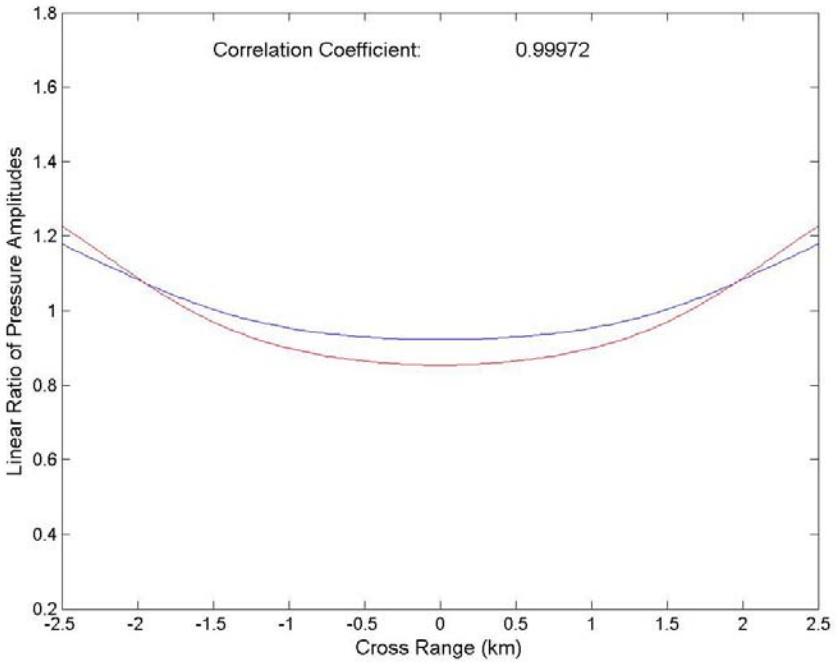

Figure 8. Line Comparison of Ratio of Modal Energies at 5km (mode 1, 150 Hz, 0^o soliton angle).

For every mode analyzed at this soliton angle, the magnitude of ratios deviation from unity is larger for the analytical model than for the PE model. This indicates that the analytical model consistently predicts a larger amount of mode coupling. Again, it is unclear if this is due to limiting assumptions of the theory or numerical issues with the PE model. The percent that the RME deviation from unity is larger for the analytical model than for the PE model for each mode at a 0^o soliton angle are tabulated in Table 1. Of note is the value for mode 5, which is almost twice as large as its nearest value 8% for mode 1. Table 2 contains the correlation coefficients at each mode analyzed at a 0^o soliton angle. The data compiled in Tables 1 and 2 indicates that the predictions produced by the analytical model are reasonably consistent with the PE model for the 0^o soliton angle case.

Soliton Angle	Percent Larger			
	Mode 1	Mode 2	Mode 4	Mode 5
0	7.99	6.57	3.61	15.27

Table 1. Maximum Percent that the Analytical RME Deviation from Unity is Greater than the PE RME Deviation From Unity

Soliton Angle	Correlation Coefficient			
	Mode 1	Mode 2	Mode 4	Mode 5
0	0.9997	0.9757	0.9347	0.8165

Table 2. Correlation Coefficients for Perturbed/Unperturbed Linear Ratios at 5 km.

2. Comparison of Analytical Model with the PE Model for a Soliton at Varying Orientations to the Main Direction of Acoustic Propagation

A surface plot of the RME is used in this section to compare the analytical model with the PE model predictions at varying soliton angles. Figures 9 and 10 are the RMEs for mode 1, 150 Hz, at a 20^o soliton angle produced from the PE model and the analytical model, respectively. Just as in the case for the 0^o soliton angle, the 20^o soliton angle causes a striation pattern made up of focusing and defocusing regions in the RME field after the soliton. The patterns are due to vertical mode coupling caused by the soliton. In fact, the work of Roush (2008) showed that horizon refraction effects do not become significant until soliton angles of approximately 85^o. Therefore, since the largest soliton angle analyzed in this paper is 80^o, all of the mode coupling effects in this paper will be the result of vertical mode coupling.

The surface plots in Figures 9 and 10 correlate well over the negative values of cross range. The extra focusing region from the analytical predictions, displayed in Figure 10, indicates that the striation patterns are slightly wider as computed by the PE model, displayed in Figure 9. The oscillation in Figure 9 does not appreciably change the RME field, and therefore is not a major difference between the models for this soliton angle and mode. The correlation breaks down for the positive cross range values. In

Figure 9, the PE model predicts that a defocusing region covers the entire area, where the analytical model in Figure 10 exhibits an extra focusing region.

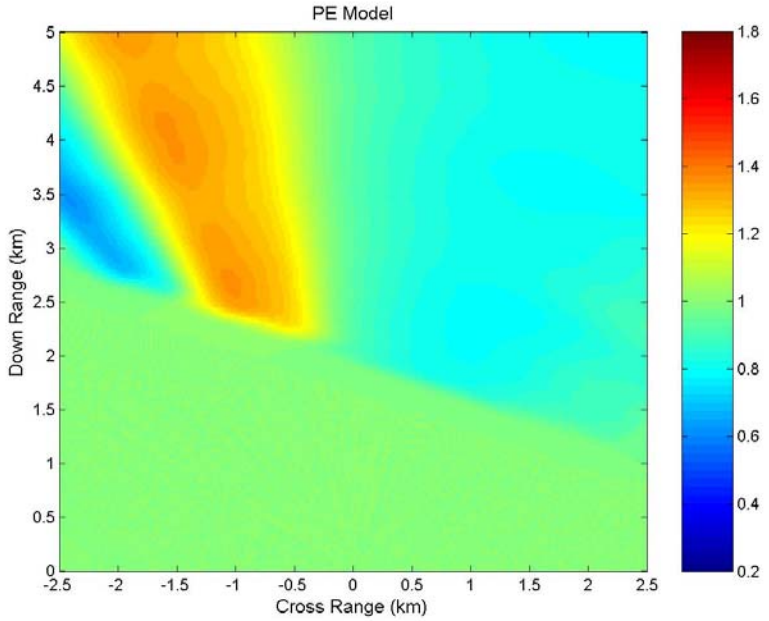

Figure 9. Ratio of Modal Energies (mode 1, 150 Hz, 20^{o} soliton angle)

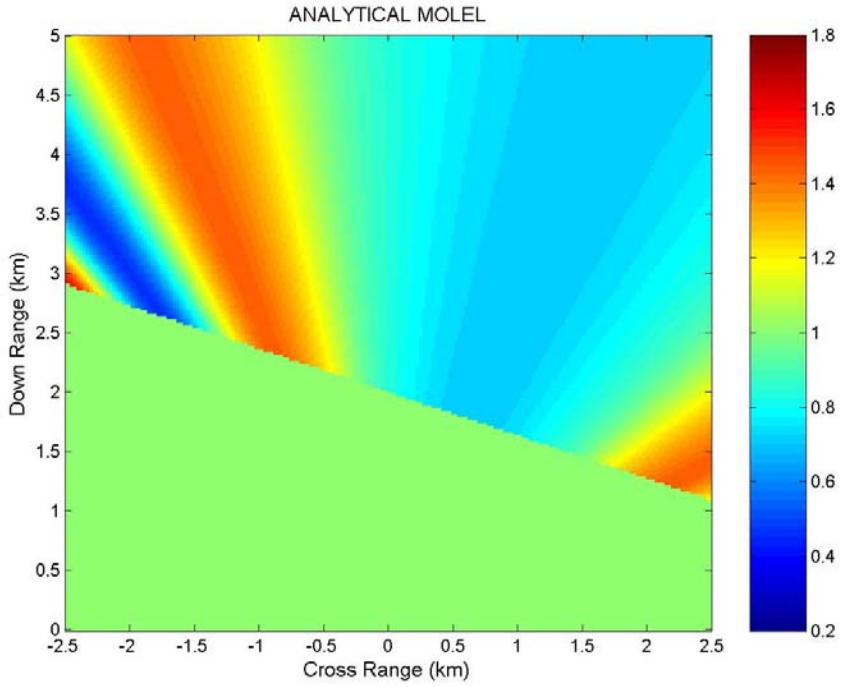

Figure 10. Ratio of Modal Energies (mode 1, 150 Hz, 20^{o} soliton angle)

Next, the 50^o soliton angle case is examined. Figures 11 and 12 are the RME distributions from the PE model and the analytical model, respectively, for mode 1, 150 Hz, and a 50^o soliton angle. A comparison between Figures 11 and 12 does show that the models continue to correlate well. The size of the striation patterns actually correlate better over the entire spectrum of cross range values. However, the difference in the magnitude of the RMEs deviation from unity is more pronounced for this soliton angle. The analytical model still shows a defocusing region in the positive cross range area that is not present for the PE model, but this region is beyond the 60^o boundary condition of the PE. The PE does not produce accurate results at an angle greater than 60^o from the vertical due to limited angular extent of the source. The oscillation in the focusing region of Figure 11 is more pronounced for this angle than for the 20^o soliton angle but is not as significant to the overall look of the field as for the 0^o soliton angle. The oscillation is also occurring in different areas of the RME field for each soliton angle. All of the above considered, the models still correlate well.

Overall, from looking at the surface plots of the RMEs presented here, the analytical and PE numerical predictions appear to correlate well. The two models are not expected to produce point wise accurate results. Instead, the goal is to confirm that the two methods produce the same general shape and magnitude of RME. From the above surface plots, this goal appears to have been reached. Surface plots of the RME at 10^o soliton angle increments from 0^o to 80^o at mode 1, 2, 4, and 5 were evaluated as part of this analysis. There, results were consistent with the conclusions presented for the surface plots shown above. One difference of note is that the oscillation contained within the striation patterns for the PE model became more significant in the appearance of the RME field with increasing mode number.

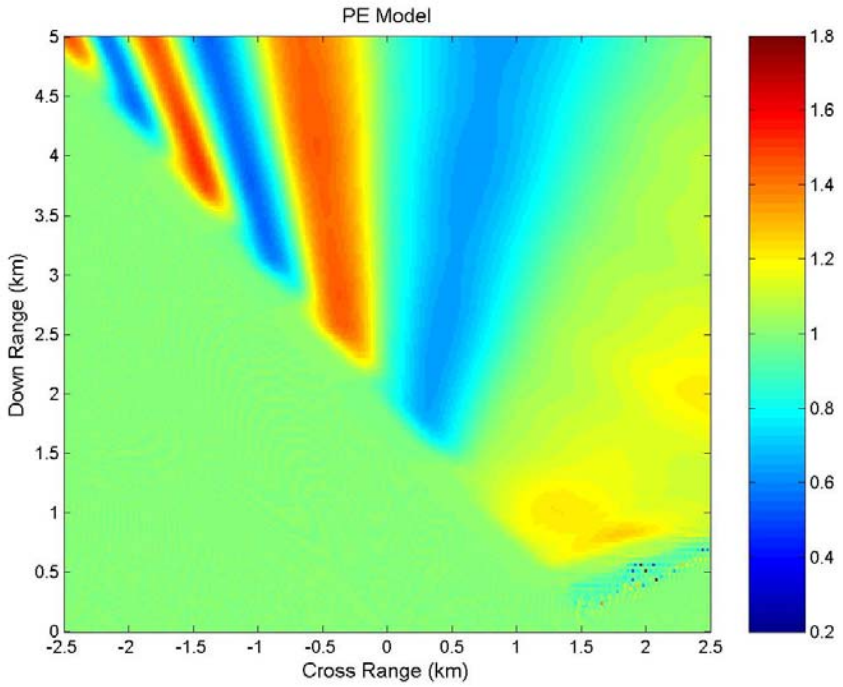

Figure 11. Ratio of Modal Energies (mode 1, 150 Hz, 50^{o} soliton angle)

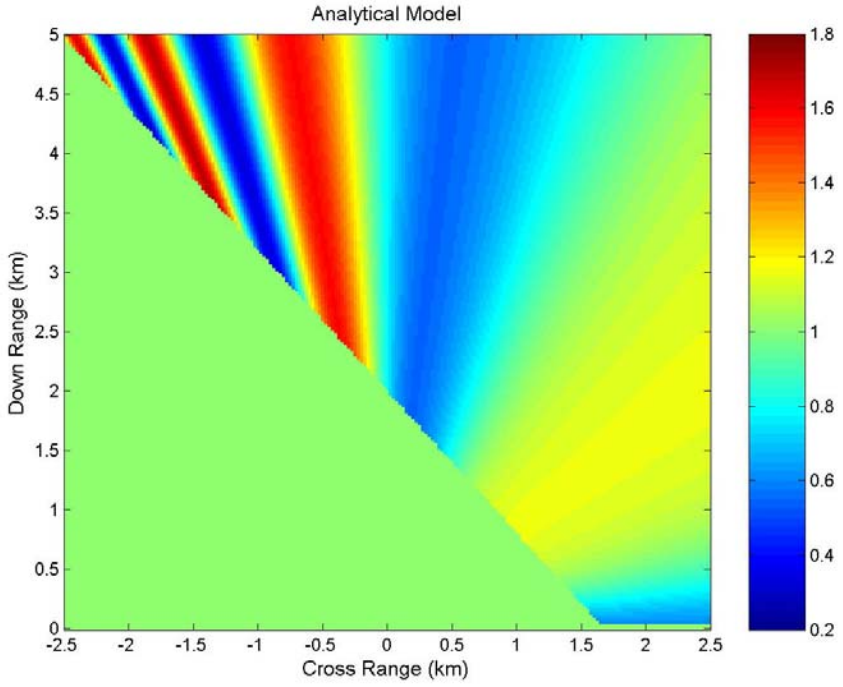

Figure 12. Ratio of Modal Energies (mode 1, 150 Hz, 50^{o} soliton angle)

As for the zero soliton angle case, a quantitative look at the RME is taken by looking at their values for a fixed down range value. Figures 13 and 14 show how well the PE model and analytical model correlate for the 20^o and 50^o soliton angles. The correlation ratios are 0.9893 and 0.8758, respectively. However, a trend can be seen in the line comparisons. As the soliton angle increases, the difference in the magnitude of the RMEs deviation from unity increases. The difference in the magnitudes is most likely due to two possible causes. There may be a process that the analytical model does not account for that is causing less vertical mode coupling to occur than expected. Or, the method in which the analytical model and the PE model account for the initial conditions is different.

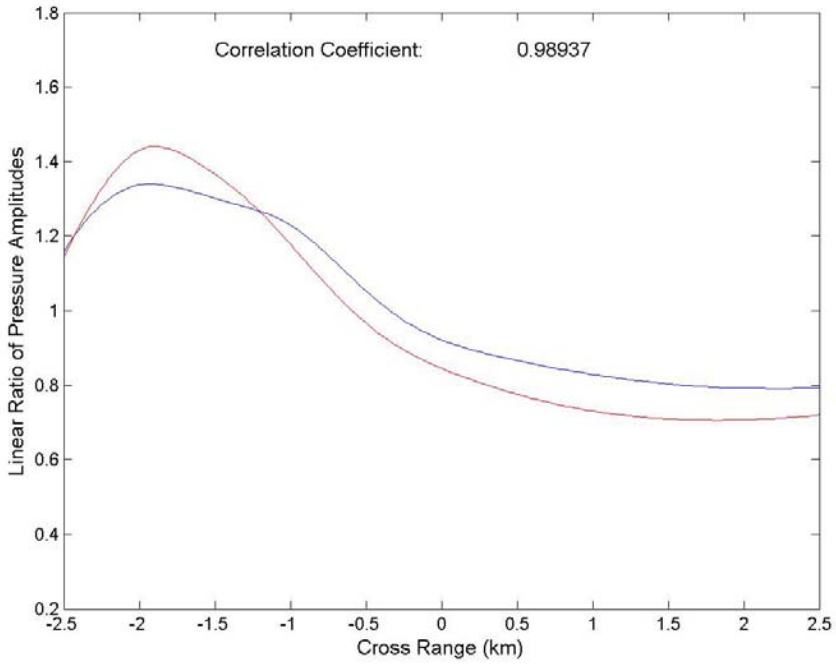

Figure 13. Line Comparison of the Ratio of Modal Energies at 5km (mode 1, 150 Hz, 20^o soliton angle).

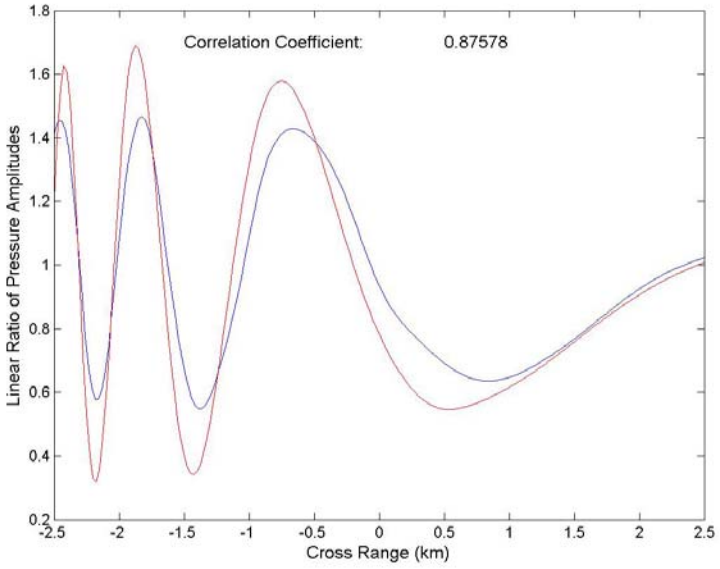

Figure 14. Line Comparison of the Ratio of Modal Energies at 5km (mode 1, 150 Hz, 50^{o} soliton angle).

Table 3 lists all of the correlation ratios for the varying soliton angles for modes 1, 2, 4, and 5. Mode 3 was not used for comparison due to the small amount of acoustic energy initially put into that mode. With the exception of mode 4 at a soliton angle of 80^{o}, all of the correlation values are greater than 75%. This value can be explained by referring to Figure 15. The large blue spike is the PE RME between -1 and -0.5 km cross range and is caused by the presence of the soliton. When the PE calculates the RME, it uses the unperturbed vertical mode shapes. However, along the soliton crest, the mode shapes are distorted due to the change in sound speed profile. The PE model assumes the same mode shape at the soliton to determine the RME due to the complex calculation that would be required to calculate the exact mode shape at the soliton. This assumption is justified considering the small width of the soliton (100m) compared to the range scale being used in the model (5 km) and the reduced run time required to run the PE. However, this assumption is the cause for the divergence between the PE model and analytical model right at the soliton (i.e., the large blue spike). This means that the models do agree to a high degree of certainty in the geometric location of the vertical mode coupling. However, the modal decomposition of the PE field is not strictly valid in the vicinity of the soliton.

Soliton Angle	Correlation Coefficient			
	Mode 1	Mode 2	Mode 4	Mode 5
0	0.9997	0.9757	0.9347	0.8165
10	0.9810	0.9810	0.9046	0.9128
20	0.9894	0.9831	0.8183	0.8850
30	0.9715	0.9652	0.8712	0.8294
40	0.9509	0.9647	0.8684	0.8107
50	0.8758	0.9281	0.8155	0.7499
60	0.8191	0.9103	0.8187	0.8417
70	0.8552	0.9331	0.7985	0.8262
80	0.8438	0.8028	0.2828	0.7671

Table 3. Correlation Coefficients for Perturbed/Unperturbed Linear Ratios at 5 km

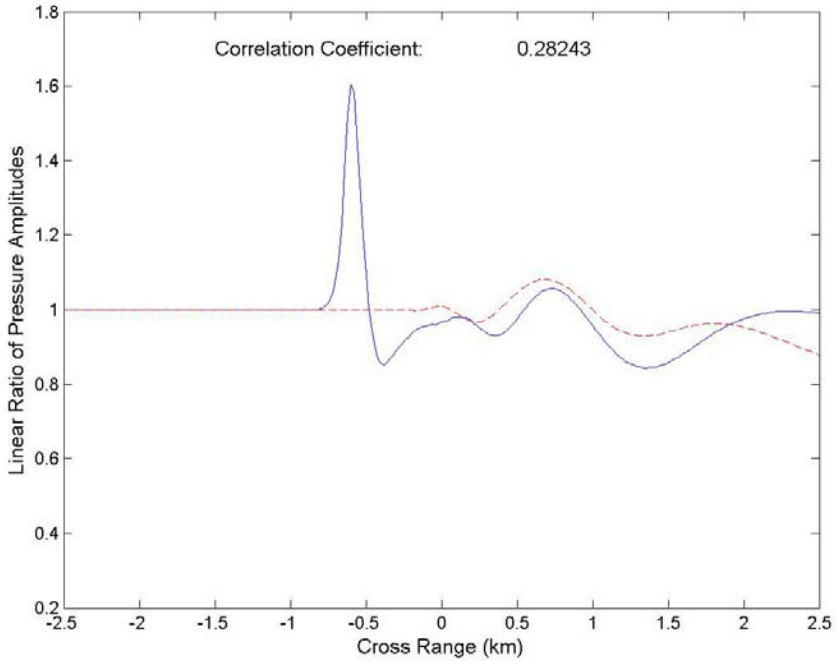

Figure 15. Line Comparison of the Ratio of Modal Energies at 5km (mode 4, 150 Hz, 80^{o} soliton angle).

For the 20^{o} soliton angle, the magnitude of the deviation from unity for the analytical model is 7.52% larger than for the PE model. As can be seen in Figures 8, 13, and 14 for mode 1, there is a good correlation between the magnitudes of the ratios. Table 4 shows how much larger the magnitude of the RME is for the analytical model

than for the PE model at the maximum difference. Overall, Table 4 shows an increase in the difference between the magnitudes for increasing soliton angles. Mode 5 also has larger differences in magnitude than the other modes. This could be a result of the low initial energy deposited into that mode due to the source depth. Figures 13 and 14 are good examples of the average mismatch in magnitude of the RMEs with values of 7.52% and 15.92%. Figure 16 is an example of the more extreme mismatch, with the analytical model RME deviation from unity more than 40% larger than the PE model RME deviation from unity.

Soliton Angle	Percent Larger			
	Mode 1	Mode 2	Mode 4	Mode 5
0	7.99	6.57	3.61	15.27
10	8.31	9.88	6.60	9.93
20	7.52	13.77	8.99	26.70
30	7.58	15.02	8.19	24.08
40	9.12	11.43	8.28	41.82
50	15.92	11.79	6.62	41.99
60	18.73	11.67	7.81	34.19
70	14.51	24.99	7.73	17.92
80	12.52	14.23	2.34	24.95

Table 4. Maximum Percent that the Analytical RME Deviation from Unity is Greater than the PE RME Deviation from Unity

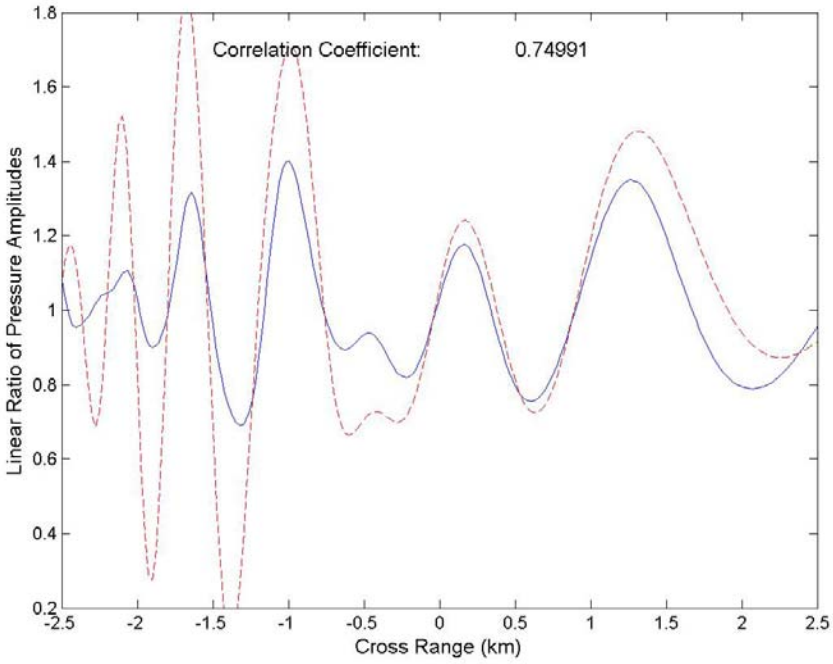

Figure 16. Line Comparison of the Ratio of Modal Energies at 5km (mode 5, 150 Hz, 50 soliton angle).

3. Conclusions

In this section, we have analyzed the correlation between the RMEs produced from the results of the analytical and PE models for sound propagation through a single soliton. Through those analyses, we have shown that the analytical model does produce results consistent with the PE model over the soliton angles and mode numbers analyzed. For example, both models produce RME fields with striation pattern of comparable size, shape, and magnitude. However, some limitations have also been discovered. For certain mode numbers and soliton angles, the RME deviations from unity are more than 49% larger for the analytical model than for PE model. The correlation coefficients for the geometric alignment of the striation pattern also dropped to as low as 0.7671. These differences in the results do not have a discernible trend in which to predict conditions where large errors would occur. The PE model also contains patterns in the striation patterns that oscillate as a function of range from the source for a given angle of acoustic

propagation that did not occur in the analytical model. These limitations make point wise agreement of solutions unlikely. However, the analytical model is sufficient at predicting the same trends and general behavior as produced by the PE model.

B. COMPARISON OF ANALYTICAL MODEL WITH THE PE MODEL PREDICTION FOR MODE COUPLING RESONANCE BEHAVIOR

In this section, to determine if the PE model follows the mode coupling resonance behavior called for by the theory, a comparison is made between the PE model and the analytical model. First, the theory behind why the resonance occurs will be reviewed. Then, the conditions for the comparison will be explained. Finally, the results from the PE model will be analyzed to determine how well they compare with the analytical prediction.

1. Theory Behind the Mode Coupling Resonance Behavior

According to Colosi (2008) the vertical mode coupling should exhibit a resonance condition dependent on the soliton width (Δ) and the frequency of the acoustic wave (ω). Colosi (2008) showed that the modal energy after propagation through a soliton is

$$\left|A_n(R)\right|^2 = \left[\left|A_n(0)\right|^2 + 2\sqrt{\pi}\sum_{m=1}^{N} A_{mn}(0) Z_{mn}\Delta_f \exp\left[\frac{-k_{mn}^2\Delta_f^2}{4}\right]\sin(k_{mn}r_o)\right] e^{-2\alpha_n R}, \qquad (51)$$

where $\left|A_n(0)\right|^2$ is the initial mode energy, A_{mn} is the initial mode amplitude matrix, Z_{mn} is the matrix that incorporates the depth structure of the soliton for modes m and n, k_{mn} is the beat wavenumber, and r_o is the distance from the source to the soliton. At small and large values of Δ, the second term on the right hand side of Equation 51 is driven to zero. Therefore, a resonance condition is reached when $\Delta \simeq \sqrt{2}/k_{mn}$. Work done by Colosi and Flatte (2008) showed that the RMS variation in mode energy caused by one soliton, averaged over a span of r_o values, per meter of internal displacement, is represented by

$$\Gamma_n(\omega,\Delta) = \frac{2\sqrt{\pi}}{|\zeta_o|}\left\langle\left(\sum_{m-1}^{N}\frac{A_{mn}(0)}{\left|A_n(0)\right|^2} Z_{mn}\Delta_f \exp\left[-\frac{k_{mn}^2\Delta_f^2}{4}\right]\sin(k_{mn}r_o)\right)^2\right\rangle_{r_o}^{1/2} \qquad (52)$$

Note that here Δ_f is used to denote the effective width of the soliton in the direction of acoustic propagation other than normal to the soliton. This expression was used to

produce Figure 17, which was used to determine the approximate width of the soliton when the resonance occurs. Note that Figure 17 is averaged over a set of r_o values. Also, the water depth used to produce Figure 14 was 100 m which is the same water depth used by the PE, but the source is located at 90 m rather than the 50 m used by the PE. Therefore, the Δ determined from Figure 17 is not expected to yield exact results for Δ at the resonance but will provide a good estimate that can be used to determine if the PE is consistent with the analytical model.

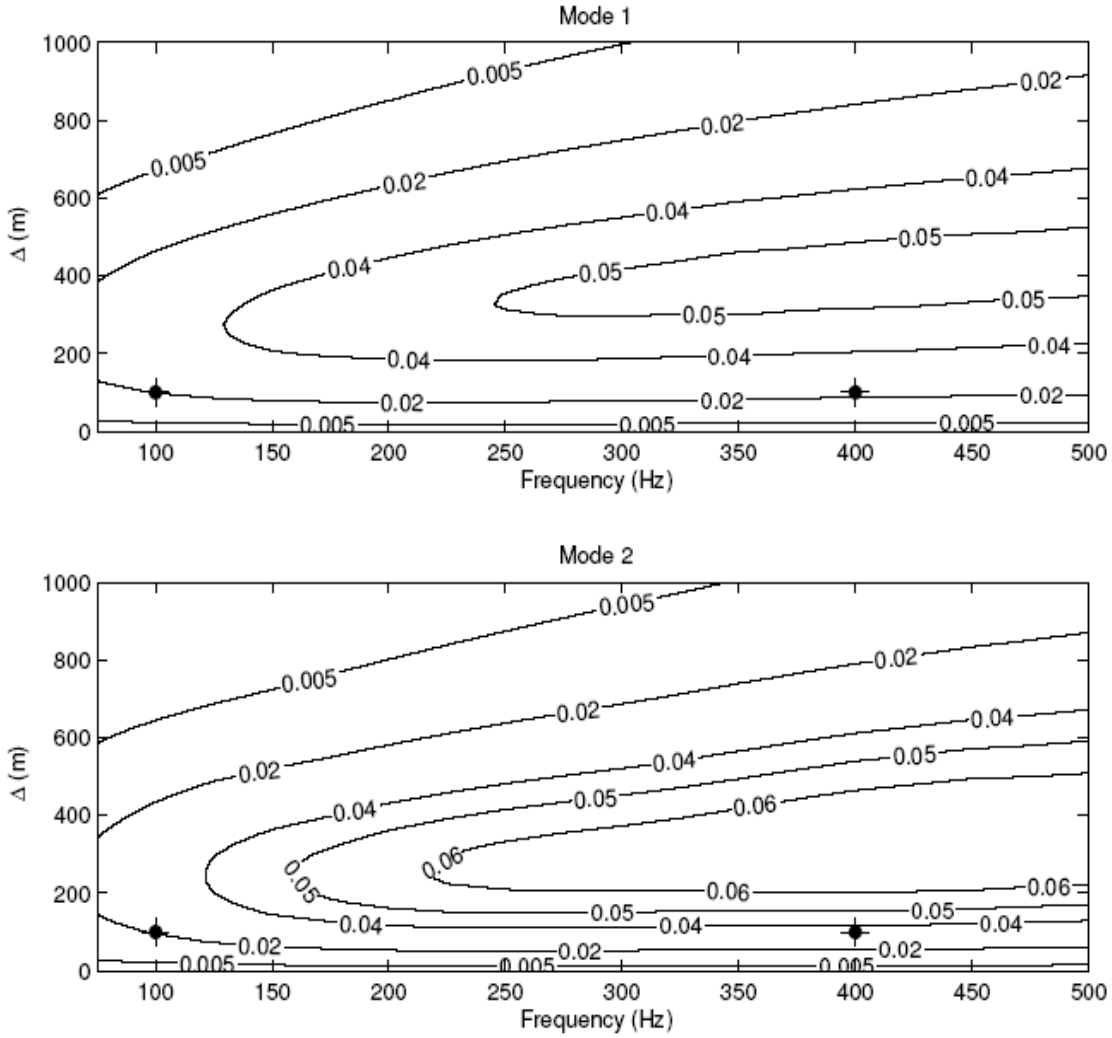

Figure 17. Contours of RMS Relative Mode Energy Fluctuation per Meter of Soliton Displacement, $\Gamma_n(\omega,\Delta)$ (m^{-1}) for a 100 m Water Depth Canonical Shallow Water Ocean Waveguide as Described by Colosi and Flatte (2008).

2. PE Mode Coupling Resonance

The theory suggests that Figure 17 above can be used to determine the approximate location of the vertical mode coupling resonance based on the frequency and width of the soliton. Therefore, the PE model can be used to validate the analytical model by varying the soliton width and/or acoustic frequency to determine if the resonance occurs, as suggested by the theory. In this analysis, a constant acoustic source frequency of 150 Hz is used, and the soliton width in the PE model (Δ_{PE}) is varied between 50 m and 500 m in increments of 50 m. Note that the results for the 200 m Δ_{PE} are not used due to a processing problem that could not be resolved. From Figure 17 above, the vertical mode coupling resonance for an acoustic signal at 150 Hz should occur at an approximate soliton width of 300m for mode 1 and 250m for mode 2. Figure 18 shows the RMEs at a fixed down range value of 5 km for varying widths. All of the solitons are oriented at a soliton angle of 45^o. A similar plot is shown in Figure 19 for mode 2. From Figure 18, it is apparent that a resonance condition does exist. In fact, one resonance condition exists for each focusing and defocusing region in both modes. The Δ_{PE} at resonance for the defocusing region at 1 km cross range in Figure 18 is 250 m. That is less than a 17% error from the 300 m width predicted from Figure 17.

Note from Figures 18 and 19 that the values of the Δ_{PE} at the resonances are not the same for each focusing and defocusing region. The different Δ_{PE} at resonance is caused by the spherical wave fronts intersecting the soliton at different angles along its length. For this analysis, the acoustic source is a point source centered at 0 km cross range and 0 km down range. The soliton is oriented at a 45^o angle from the horizontal and centered at a point located at 0 km cross range and 2 km down range. The angle between the path the acoustic energy takes and the soliton changes along the length of the soliton. Therefore, the distance the acoustic energy travels while crossing through the soliton changes along the length of the soliton.

Due to the symmetry along its axis, the change in distance through the soliton can be accounted for with an effective soliton width ($\Delta_f = \Delta / \cos(\theta_f)$) (Colosi, 2007). The

resonance at 1 km cross range is oriented such that the angle between the acoustic path and the normal to the soliton is zero. Therefore, the Δ_f is equal to the Δ_{PE}. For the remaining resonances, since the soliton width read from Figure 17 is the Δ_f and the width read from Figures 18 and 19 are the actual widths of the soliton, to make a comparison the actual widths of the soliton must be converted to effective widths. For the focusing region located at about -750 m cross range, the angle between the path of propagation and the normal to the soliton is about 60^o. Therefore, the effective soliton width is

$$\Delta_f = \Delta / \cos(\theta_f) = 150m / \cos(60.26) = 302m . \tag{53}$$

The percent difference from the 300 m that was predicted from Figure 17 is less than one percent. The effective soliton widths for all of the resonance shown in Figures 18 and 19 are tabulated in Table 5. All of the effective soliton widths are within 20% of the predicted soliton width except two, which are located at -1.7 km and -2.25 km cross range in mode 2. The percent errors for these soliton widths are about 70 and 40 percent, respectfully. Overall, the results do show that the PE model produces results that are consistent with the analytical model.

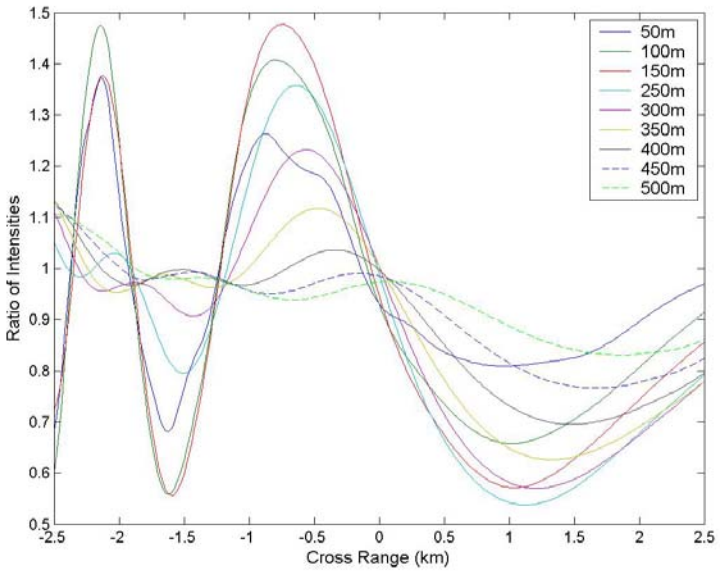

Figure 18. Comparison of Mode Coupling for Different Soliton Widths at 5 km (mode 1, 150 Hz, 45 soliton angle)

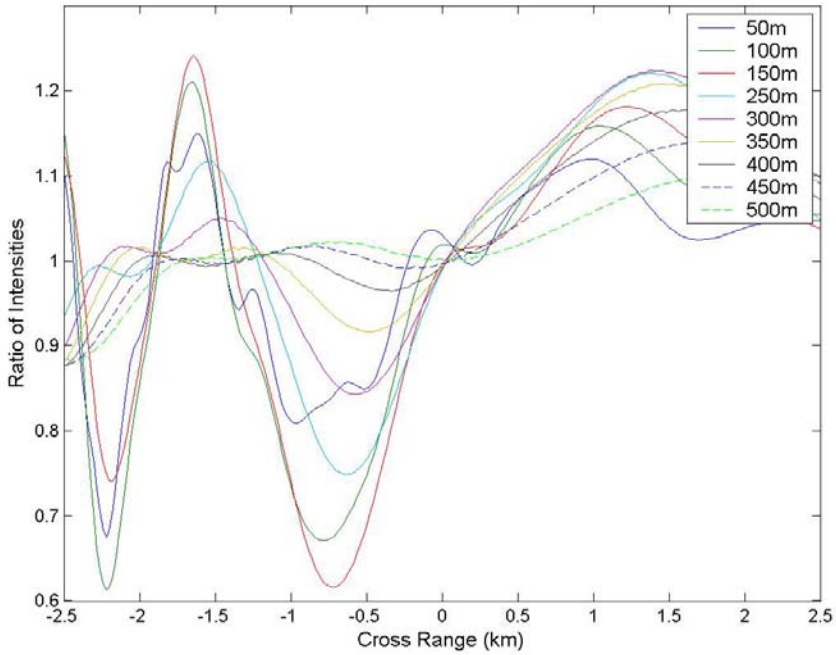

Figure 19. Comparison of Mode Coupling for Different Soliton Widths at 5 km(mode 2, 150 Hz, 45 soliton angle)

	Mode 1				Mode 2		
Cross Range	ΔPE	Δeff	% Diff	Cross Range	ΔPE	Δeff	% Diff
1 km	250	250	16.67%	1.4 km	275	296	18.40%
-0.75 km	150	302	0.67%	-0.75 km	150	296	18.40%
-1.65 km	125	348	16.00%	-1.7 km	150	424	69.60%
-2.2 km	100	335	11.67%	-2.25 km	100	335	34.00%

Table 5. Effective Soliton Width for each Resonance Shown in Figure 18 and 19

3. Conclusions

In this section, the mode coupling resonance condition for the PE was compared to the analytical predictions for varying soliton widths. The results tabulated in Table 5 show that the PE agrees well with the theory for mode 1. However, the PE begins to differ considerably from the analytically predicted values for mode 2. The fact that one mode agrees and the other mode does not is not enough data to really determine how well

the models correlate as a whole. Further analysis should be conducted to include more modes and reproduce Figure 17 using the correct initial conditions.

C. COMPARISON OF THE ANALYTICAL MODEL WITH THE PE MODEL FOR MULTIPLE SOLITONS AT VARYING ORIENTATIONS

In this section, the results of the PE model and analytical model will be compared for the purpose of validating the results of the analytical model for a soliton packet. As in Section A, the comparison will be based on how well the RME from each model correlate with the other. This approach is still valid for soliton packets, since both models still assume that the acoustic variability introduced by the soliton packet is confined to the RME.

The same criteria will be used to measure the correlation between models for the soliton packet case as for the single soliton case. The first criteria will be a correlation coefficient, which is a measure of how well the different regions of mode coupling align geometrically (Rodgers and Nicewander, 1988). The second criteria will be a comparison of the magnitude of the RME at the maximum difference between them.

1. Comparison of the Analytical Model with the PE Model for a Soliton Packet Perpendicular to the Main Direction of Acoustic Propagation

In this section, the models will be compared for the case where the soliton packet is oriented at a 0^o soliton angle. As noted in Section A, the soliton angle is measured from the horizontal plane which is perpendicular to the main direction of acoustic propagation. The soliton packet is composed of three solitons, each 100 m in width and separated by 500 m. The vertical displacement of the solitons from the first soliton to the third is 10 m, 9 m, and 8 m, respectfully. In this notation, a positive vertical displacement of the solitons is in the positive z-direction, which is positive with increasing depth (down direction). The 0^o soliton angle case is ideally the simplest case since the majority of the acoustic energy will be incident at a near normal angle to the soliton where the mode coupling occurs entirely in the vertical plane (Colosi, 2008). As in the single soliton case a surface plot of the RME for each model will be compared qualitatively for

geometric orientation and magnitude. A line plot of the RME at 5 km from the source will be used to make a quantitative comparison of the geometric orientation and magnitude of the RME.

Figures 20 and 21 are surface plots of the RMEs produced by the PE model and the analytical model. In Figure 20, the end of the soliton packet is easily identified by the change in the magnitude of the RME at 2 km down range from the source. For the analytical predictions, all of the effects of the soliton packet are summed and applied at the leading edge of the soliton packet (Colosi, 2008). Therefore, the RME field produced by the analytical model is not valid until after the final soliton in the packet. To identify this point, a line has been superimposed onto the RME field in Figure 21 to identify the end of the soliton packet. The PE model also has areas where the RME field is not valid. At the interface of each individual soliton the PE assumes that the same unperturbed vertical mode shapes exist across the solitons. This is not the case, since the soliton distorts the mode shapes across their interface. Therefore, the RME are not valid in parts of the field where a soliton is located. However, this assumption is valid over most of the field ,due to the small area an individual soliton covers, compared to the rest of the field and the faster runtime the program gains by not attempting to recalculate the mode shapes. For the purpose of this analysis, the models will only be compared for the part of the field after the last soliton in the packet.

The RME fields produced by the PE model in Figure 20 and the analytical model in Figure 21 have the same general shape. Both fields consist of striation pattern symmetric about the center. The oscillation in the focusing region of Figure 20 does significantly affect the appearance of the field. The width of the focusing regions in Figure 20 also does not appear to be as wide as the corresponding regions in Figure 21. This is apparent by the fact that Figure 20 has two focusing regions per side but Figure 21 only has one. Also, the defocusing regions in Figure 21 at about ±2.5 km cross range is much more intense than in Figure 20.

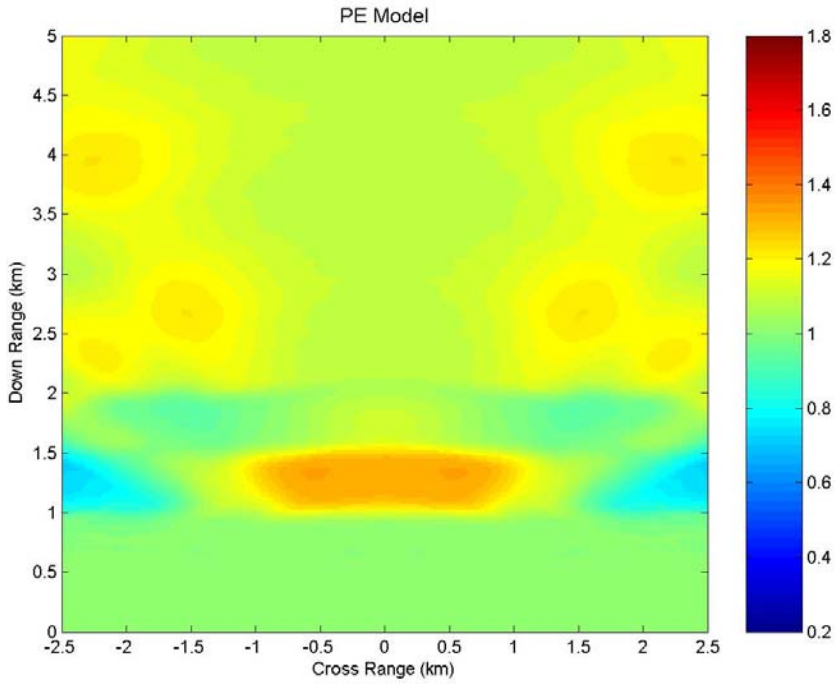

Figure 20. Ratio of Modal Energies (mode 1, 150 Hz, 0^o soliton angle)

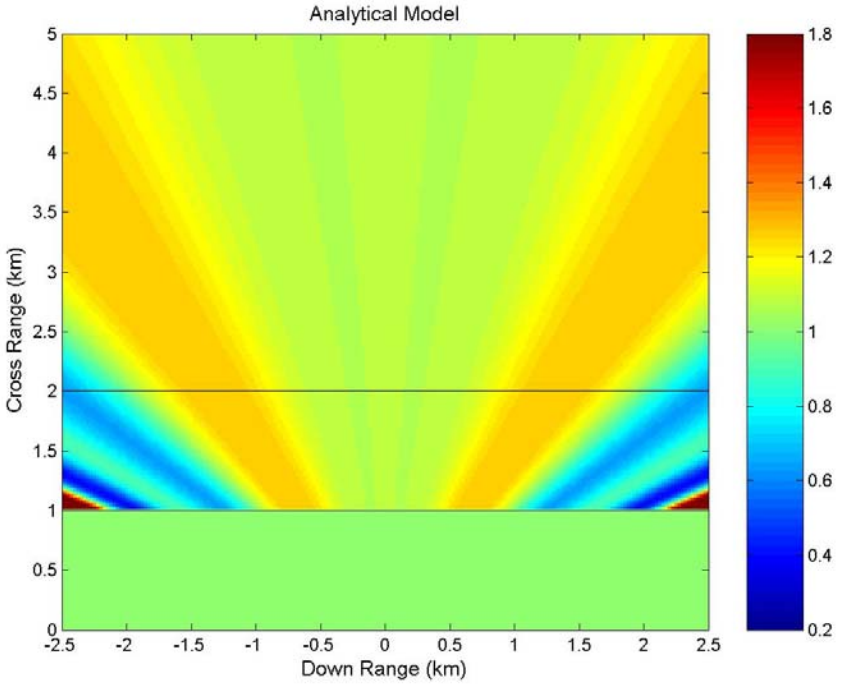

Figure 21. Ratio of Modal Energies (mode 1, 150 Hz, 0^o soliton angle)

A comparison of the PE model and analytical model for surface plots corresponding to modes 2, 4, and 5 were performed with similar results. However, the analysis does yield two major differences between the models. The first difference is that the RME from the PE model can vary greatly from the analytical model as a result of an oscillation within the striation pattern. The analytical model does not contain these oscillations. Figures 22 and 23 demonstrate how significantly an effect these oscillations can have on the RME field. The second difference is that the analytical model usually has a larger amount of mode coupling than the PE model. This is demonstrated by the larger magnitude of deviation form unity in the RME field for the analytical model. Both differences will be addressed again later in this paper using the correlation coefficient and by comparing the maximum difference in model amplitudes.

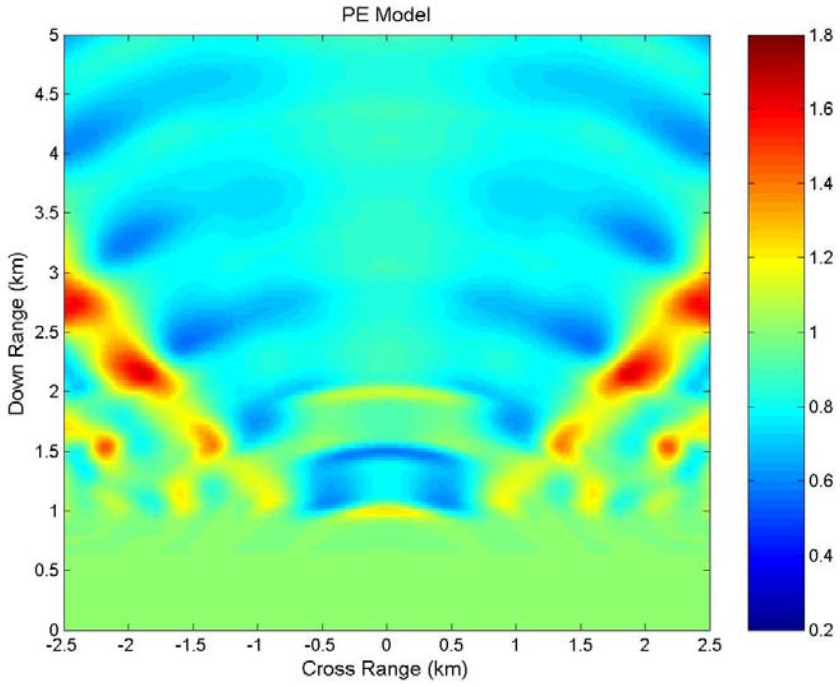

Figure 22. Ratio of Modal Energies (mode 5, 150 Hz, 0^{o} soliton angle)

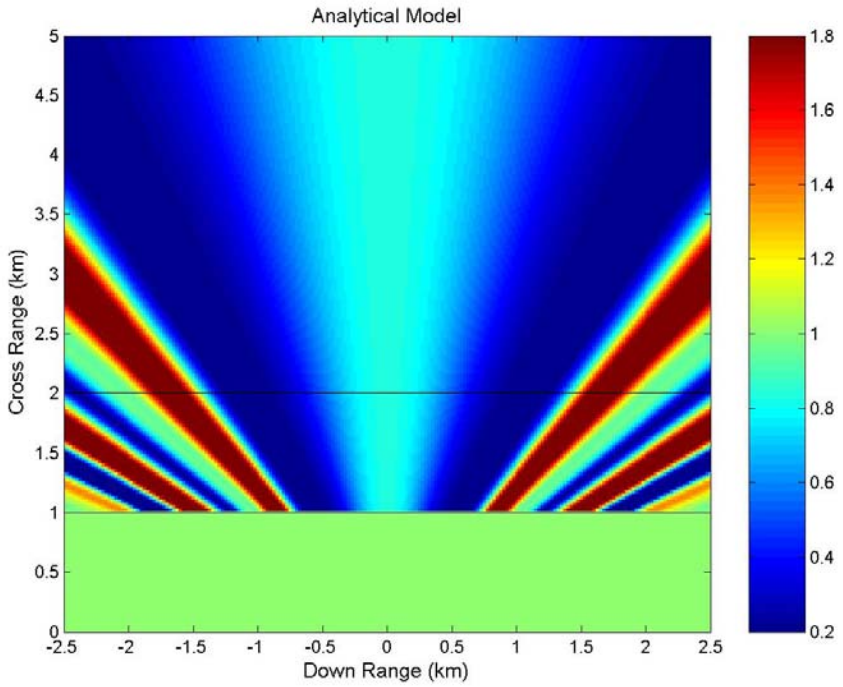

Figure 23. Ratio of Modal Energies (mode 5, 150 Hz, 0^o soliton angle)

A quantitative comparison of the correlations shall now be made by looking only at the RMEs at a specific down range value. Figure 24 is a line plot of the RMEs with the PE model in blue and the analytical predictions in red. The range for the comparison was chosen to be at 5 km to stay consistent with other line comparisons presented elsewhere in the paper. The RMEs in Figure 24 align very closely, with a small divergence at cross ranges greater than 2 km. At the maximum difference between RMEs, the RME deviation from unity is only 1.55% greater for the analytical model than for the PE model. The RMEs for this mode have a correlation coefficient of 0.9881. Therefore, for this mode computed with this soliton angle, at this rang, the analytical model produces results very consistent with the PE model. Tables 6 and 7 contain the tabulated maximum percent difference and correlation coefficients for modes 1, 2, 4 and 5 at the 0^o soliton angle. Table 7 shows that the geometric alignment of the mode coupling regions decreases with increasing mode number. Similarly, Table 6 shows that the magnitude of the RMEs deviation from unity increases with increasing mode number.

Figure 25 is the line comparison for mode 5 and is the case for the worst correlation between the models for the 0^o soliton angle.

Soliton Angle	Percent Larger (Analytical/PE)			
	Mode 1	Mode 2	Mode 4	Mode 5
0	1.55	5.69	10.25	-31.96

Table 6. Maximum Percent that the Analytical RME deviation from unity is Greater than the PE RME deviation from unity

Soliton Angle	Correlation Coefficient			
	Mode 1	Mode 2	Mode 4	Mode 5
0	0.98806	0.88611	0.7838	0.72149

Table 7. Correlation Coefficients for Perturbed/Unperturbed Ratios of Modal Energies at 5 km

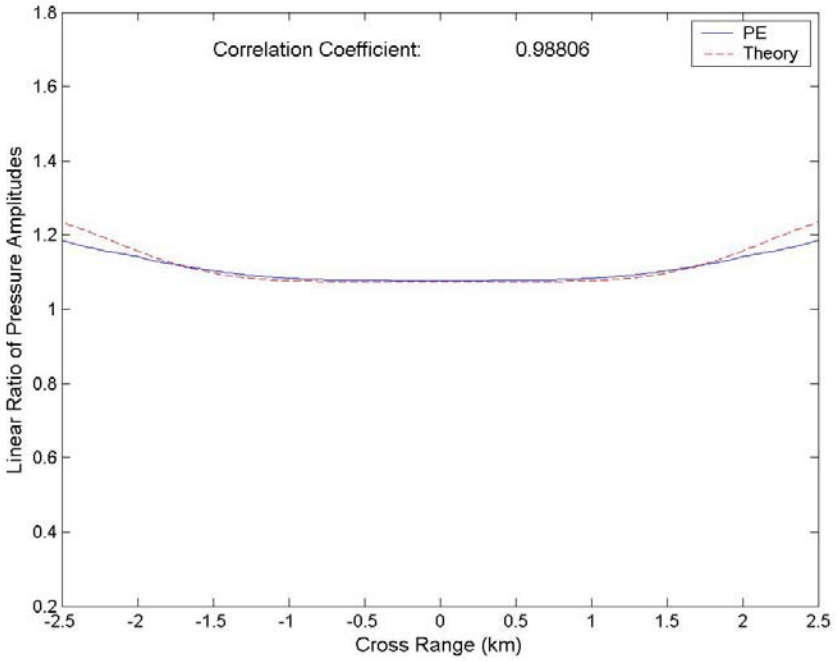

Figure 24. Line Comparison of the Ratio of Modal Energies at 5 km (mode 1, 150 Hz, 0^o soliton angle)

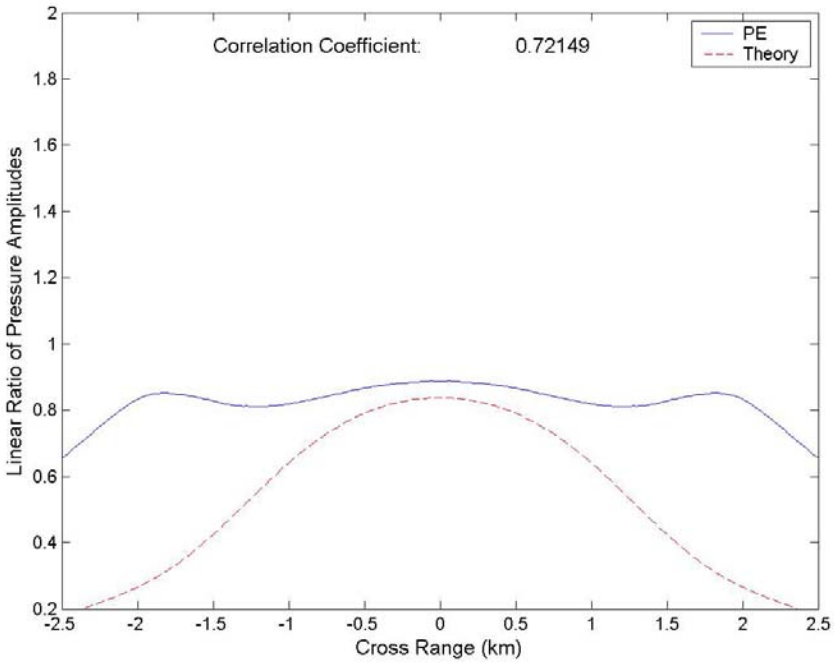

Figure 25. Line Comparison of the Ratio of Modal Energies at 5 km (mode 5, 150 Hz, 0^o soliton angle)

2. Comparison of the Analytical Model with the PE Model for a Soliton Packet at Varying Orientations to the Main Direction of Acoustic Propagation

In this section, the analytical model is compared to the PE model at varying angles of the soliton packet by looking at the surface plots of the RME. Figures 26 and 27 are the surface plots of the RMEs for mode 1, 150 Hz, at a 20^o soliton angle as produced from the PE model and analytical model, respectively. As in the case of the 0^o soliton angle, the 20^o soliton angle soliton causes striation patterns in the RME field after the soliton. The patterns are believed to be due to vertical mode coupling since the work of Roush (2008) showed that horizontal diffraction effects do not become significant until soliton angles of approximately 85^o. Therefore, for the soliton angles analyzed in this paper the mode coupling effects will be the result of vertical mode coupling. The striation patterns are made up of focusing and defocusing regions in the RME field. The size of the focusing/defocusing regions appear to be comparable, as well as the

magnitude of the ratios in each region. However, in the positive cross range section of Figure 27 there is a focusing area that is not present in Figure 26. Again, the oscillation along the focusing/defocusing regions is the biggest difference between the two models.

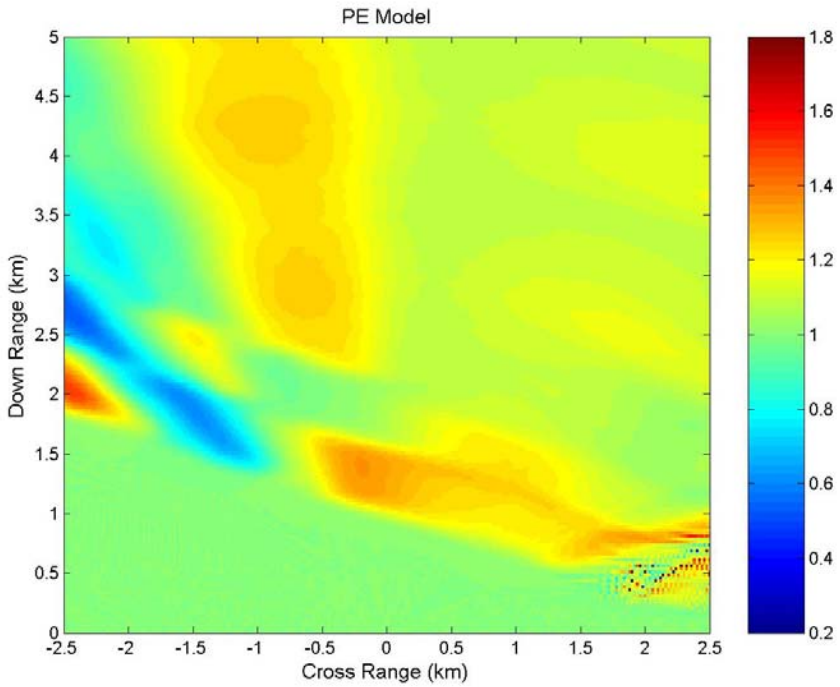

Figure 26. Ratio of Modal Energies (mode 1, 150 Hz, 20^{o} soliton angle)

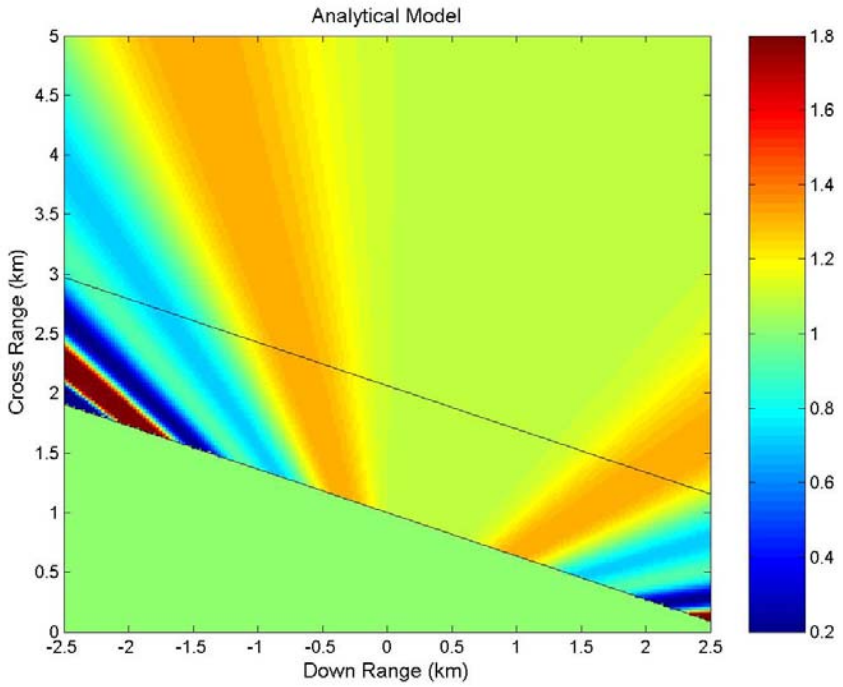

Figure 27. Ratio of Modal Energies (mode 1, 150 Hz, 20^{o} soliton angle)

Next, the soliton packet is rotated to 50^{o} to determine the effect of more grazing angles of propagation on the correlation of RME between the models. Figures 28 and 29 are surface plots of the RME for mode 1, 150 Hz, and a 50^{o} soliton angle produced by the PE model and analytical model, respectively. Both plots contain striation patterns of comparable size and with comparable magnitude of RME. The oscillations in the focusing/defocusing regions of the PE plot are less significant at this angle. This observation casts some doubt on whether the oscillation is a numerical artifact due to the use of Cartesian coordinates in the PE model. If the use of Cartesian coordinates was to blame for the oscillations, then why would the effect become less significant with an increased soliton angle? The 2-D assumption of the theory is a more likely source of the difference, and the oscillations may simply be an indication of the horizontal refraction effects. From Figures 28 and 29, we can infer that the models correlate better due to the smaller effect of the oscillations in the PE model with increasing soliton angle.

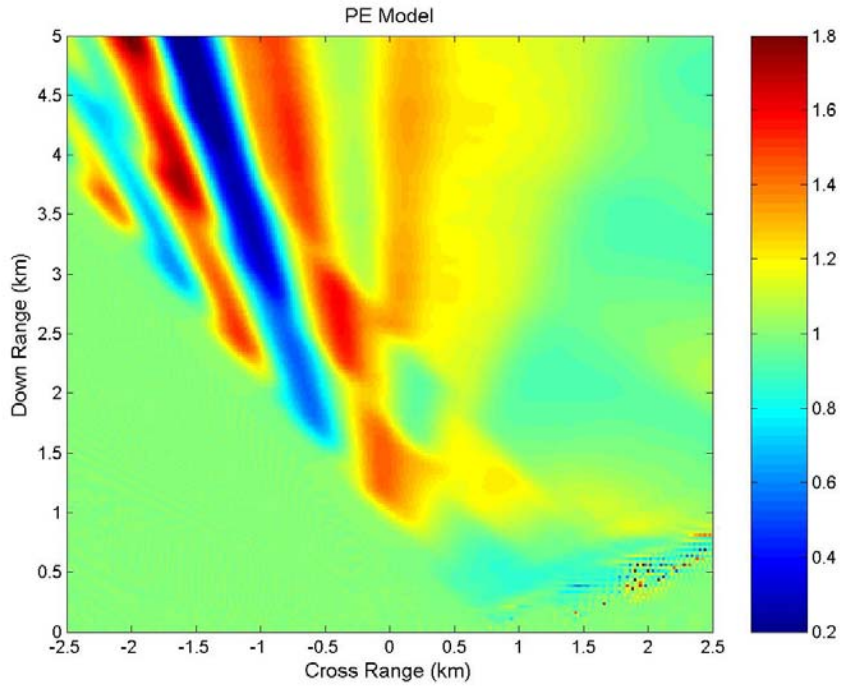

Figure 28. Ratio of Model Energies (mode 1, 150 Hz, 50^{o} soliton angle)

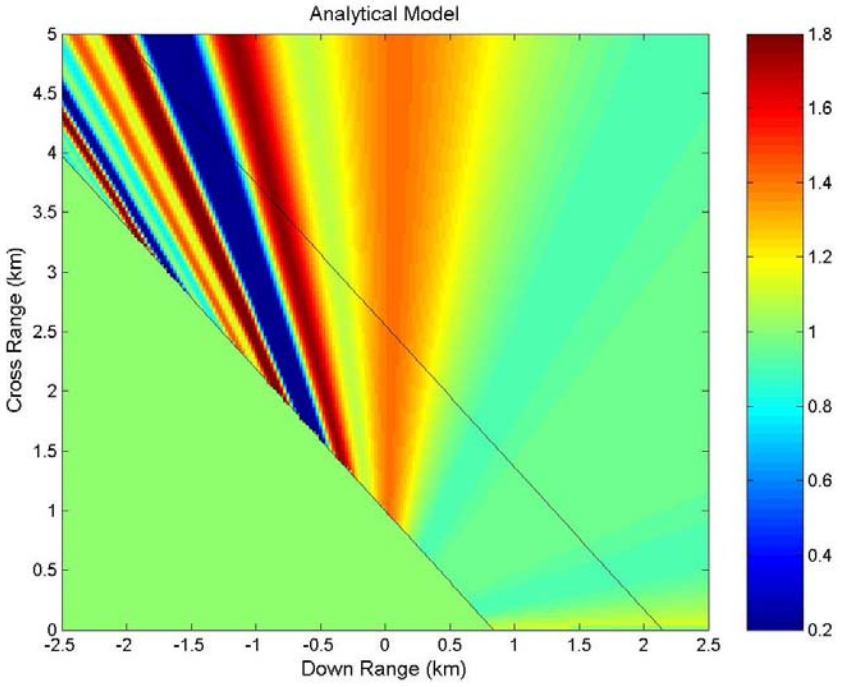

Figure 29. Ratio of Modal Energies (mode 1, 150 Hz, 50^{o} soliton angle)

A quantitative look at the RME will now be done by looking at them at a fixed down range value of 5 km. Figures 30 and 31 are the magnitude of the RME at 5 km for a 20^o and 50^o soliton angle, respectfully. The correlation coefficient for the 20^o soliton angle is 0.6678 and 0.4876 for the 50^o soliton angle. This trend does not support the early observation from the surface plots that the plots correlate better for increasing soliton angles. In fact, values tabulated in Table 8, which are the correlation coefficient for varying soliton angle at each mode analyzed, show that there is no clear trend. However, it does show that some conditions result in significant differences in the geometric alignment of the RME.

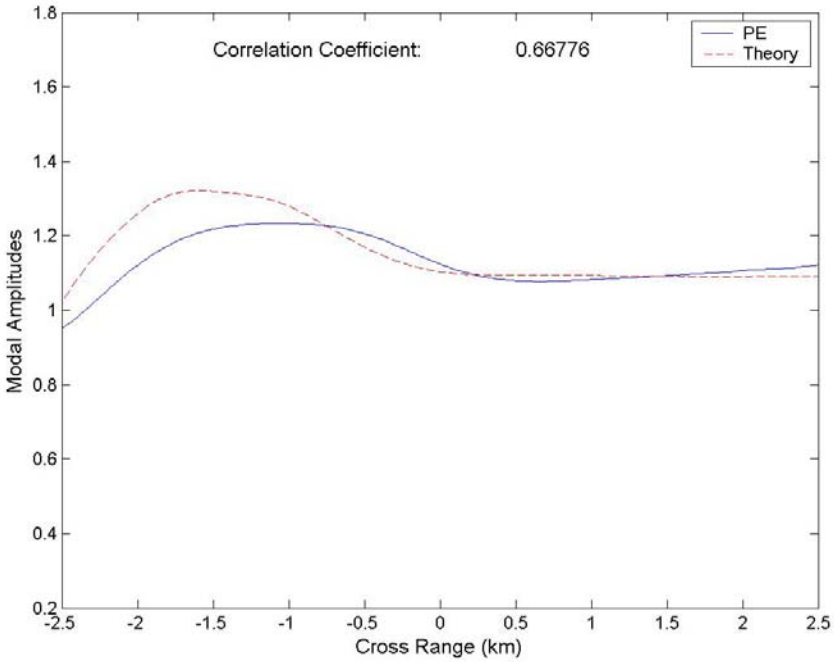

Figure 30. Line Comparison of the Ratio of Modal Energies at 5 km (mode 1, 150 Hz, 20^o soliton angle)

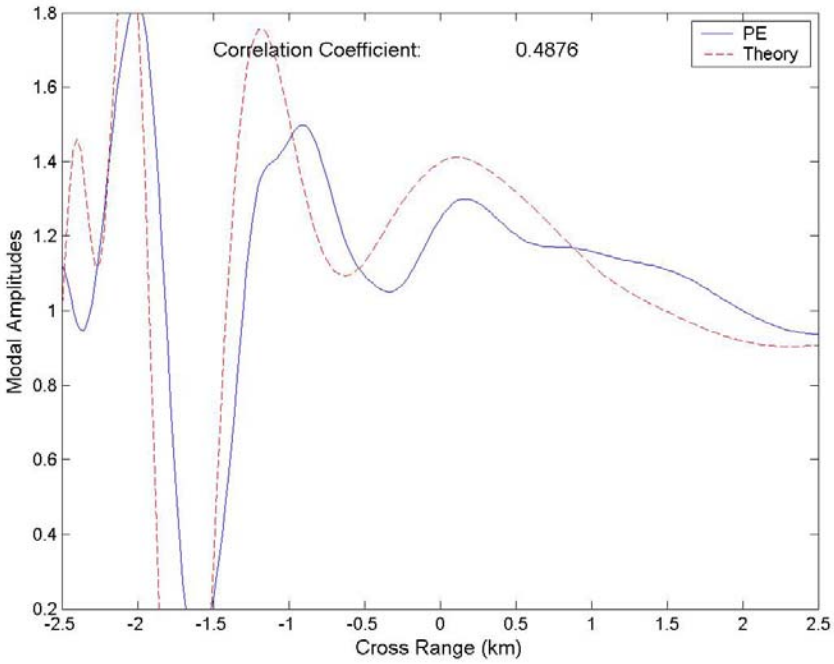

Figure 31. Line Comparison of the Ratio of Modal Energies at 5 km (mode 1, 150 Hz, 50^{o} soliton angle)

Soliton Angle	Correlation Coefficient			
	Mode 1	Mode 2	Mode 4	Mode 5
0	0.9881	0.8861	0.7838	0.7215
10	0.8796	0.9230	0.4275	0.9666
20	0.6678	0.7524	0.7295	0.9214
30	0.7897	0.3533	0.6867	0.8111
40	0.8318	0.4524	0.4485	0.6482
50	0.4876	0.6988	0.5664	0.6794
60	0.4887	0.6765	0.6342	0.9375
70	0.6025	0.5699	0.4101	0.9366
80	0.5497	0.7476	0.2828	0.9058

Table 8. Correlation Coefficients for Perturbed/Unperturbed Ratio of Modal Energies at 5 km

Since the correlation coefficient only accounts for the geometric alignment of the striation patterns and not for any differences in the magnitude of the RME within the striation patterns, we have calculated the percent that the RME deviation from unity is

greater for the analytical model than for the PE model at the maximum difference. The differences in the magnitude of the RMEs deviation from unity are tabulated in Table 9. Again, these data show that significant differences can exist between the RME for certain conditions. The analytical deviation is as much as 64% larger than the PE deviation for mode 5 with a 40^o soliton angle. Figure 32 is the line comparison for mode 5 with the 40^o soliton angle.

Soliton Angle	Percent Larger (Analytical/PE)			
	Mode 1	Mode 2	Mode 4	Mode 5
0	1.55	5.69	10.25	31.96
10	9.13	6.60	4.94	2.44
20	6.93	7.95	5.37	14.80
30	7.14	9.48	6.07	5.18
40	5.89	25.29	10.44	65.43
50	18.49	26.75	8.15	40.25
60	26.22	19.90	1.84	28.28
70	19.70	35.42	6.18	24.42
80	1.80	35.76	19.85	45.18

Table 9. Maximum Percent that the Analytical RME Deviation from Unity is Greater than the PE RME Deviation from Unity

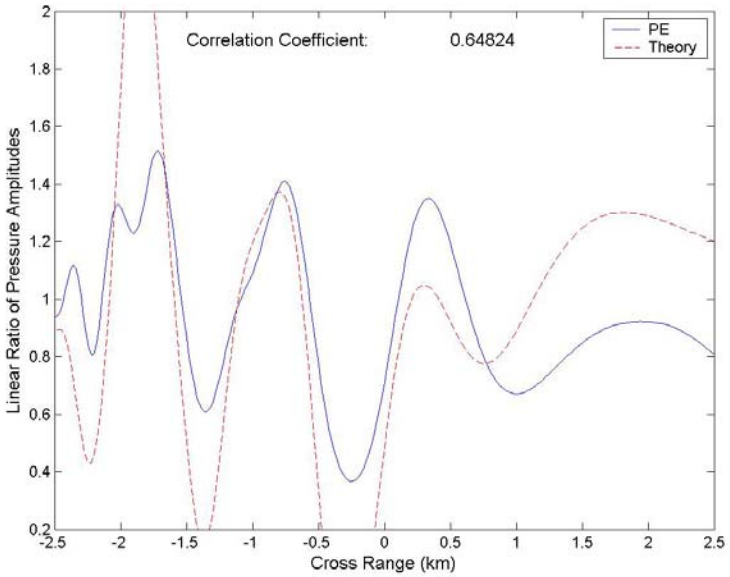

Figure 32. Line Comparison of Ratio of Modal Energies at 5 km (mode 5, 150 Hz, 40^osoliton angle)

3. Conclusions

In this section, we have analyzed the correlation between the RME produced from the results of the analytical and PE models for sound propagation through a soliton packet. Through those analyses, we have shown that the analytical model does produces results consistent with the PE model over the soliton angles and mode numbers analyzed. For example, both models produce RME fields with striation pattern of comparable size, shape, and magnitude. However, some limitations have also been discovered. For certain mode numbers and solitons, the RME deviation from unity is more than 60% greater for the analytical model than for the PE model. The correlation coefficients for the geometric alignment of the striation pattern also dropped to as low as 0.2828. These differences in the results did not have a discernible trend in which to predict conditions in which errors would occur. The PE model also contained patterns in the striation patterns that oscillated as a function of range from the source for a given angle of acoustic propagation that did not occur in the analytical predictions. These limitations make point wise agreement of solutions unlikely. However, the analytical model is sufficient at predicting the same trends and general behavior as produced by the PE model.

V. SUMMARY AND CONCLUSIONS

In this paper, the Single Scattering Analytical Model is verified through direct comparison with the 3-D implementation of a proven Parabolic Equation model, the 3DMMPE. The comparison in broken up into three parts; acoustic propagation through a single soliton, acoustic propagation through a soliton packet, and mode coupling resonance behavior caused by propagation through a single soliton. For each part, the amount of mode coupling predicted by each model is used to make the comparison. The desired result is not to show that the analytic model will produce point wise accurate results, but to show that it produces results consistent with the 3DMMPE. From the beginning, the single scattering assumptions made in the development of the analytical model were meant to produce an estimation of the mode coupling behavior. The premise of this analysis is that the assumptions made produce results that compare well with the 3DMMPE.

For acoustic propagation through a single soliton, we show that the analytical model predicts equivalent amounts of mode coupling. The analysis shows that the analytical model produces RME fields with striation pattern of comparable size, shape, and magnitude to the 3DMMPE. The analysis also determines the model's limitations. For certain mode numbers and soliton angles, the analytical model predicts as much as 49% more mode coupling than the PE model. The normalized correlation coefficients for the geometric alignment of the striation pattern can also drop as low as 0.7671. These differences in the results do not have a discernible trend in which to predict conditions where large errors would occur. Oscillations in the striation pattern present in the RME fields for the PE model contribute to the differences seen in the qualitative analysis of the RME fields and the quantitative comparison of magnitude and correlation coefficients. These limitations make point wise agreement of solutions unlikely. However, despite this limitation, the analytical model is sufficient at predicting the same trends and general behavior as produced by the 3DMMPE model.

Two more solitons were added to the acoustic field to determine its affect on the analytical model's ability to produce consistent predictions for acoustic propagation

through a soliton packet. In the analysis, we show that the analytical model still predicts equivalent amounts of mode coupling. While the predictions are not as close as for the single soliton, the model still produces RME fields with striation pattern of comparable size, shape, and magnitude to the 3DMMPE model. Again, limitations of the analytical model were identified by the analysis. For certain mode numbers and solitons, the amount of mode coupling predicted by the analytical model was as much as 60% more than what was predicted by the PE model. The correlation coefficients for the geometric alignment of the striation pattern also dropped to as low as 0.2828. These differences in the results did not have a discernible trend in which to predict conditions in which errors would occur. The oscillations in the striation patterns present in the RME field for the PE model continued to account for significant differences between the models shown by the analysis. Again, these limitations make point wise agreement of solutions unlikely, but the analysis shows that the analytical model is still sufficient at predicting the same trends and general behavior as produced by the PE model.

The mode coupling resonance behavior predicted by the analytical model is also consistent with the observed resonances in the PE model predictions. The analysis shows that the analytical model can predict which soliton width the PE model will produce a resonance for within 17% error for mode 1. For mode 2, the analytical model is less accurate at predicting the resonances of the PE model. The errors in the resonances are as high as 35%, with one outlier as high as 70%. The inconsistency in the prediction of the resonances for the different modes makes it clear that more comparisons are needed to determine just how well the analytical model can predict the resonances. Further analysis should be conducted to include more modes and the reproduction of Figure 17 using the correct initial conditions.

Further research should also be conducted to determine the source of the oscillations in the striation patterns present in the RME fields for the 3DMMPE model. The change in the oscillation with mode number and soliton angle suggest that they are a physical phenomena not accounted for by the 2-D, single scattering approximation. One possible explanation could be that they are caused by 3-D horizontal refraction effects. A comparison of the 3-D MMPE and the 2-D MMPE could resolve the oscillation to 3-D effects.

LIST OF REFERENCES

Bellman, R. (1964). *Perturbation Techniques in Mathematics, Physics, and Engineering* (Holt, Rinehart, and Winston, Inc., New York), 38–39.

Colosi, J. (2008). "Acoustic mode coupling induced by shallow water nonlinear internal waves: Sensitivity to environmental conditions and space-time scales of internal waves," J. Acoust. Soc. Am. 124, 1452–1464.

Colosi, J., and Flatte, S. (2008). Introduction to Acoustic Fluctuation Caused by Internal Waves. (Class notes, Naval Postgraduate School)

Dyson, F. (1949). "The radiation theories of Tomonaga, Schwinger, and Feynman," Phys. Rev. 75, 486–02.

Sakuri, J. (1985). *Modern Quantum Mechanics* (Benjamin/Cummings, Menlo Park, CA), 72–73.

Smith, A., and Smith, K. (1998). "Mode functions for the wide angle approximation to the parabolic equation," J. Acoust. Soc. Am. 103, 814–821.

Smith, K. (2001). "Convergence, stability, and variability of shallow water acoustic predictions using a split-step Fourier parabolic equation model," J. Comp. Acoust. 9, 243–285.

Smith, K. (2005). Sound Propagation in the Ocean. (Class notes, Naval Postgraduate School).

Smith, K., and Colosi, J. (2008). "Effects of solitons on acoustic energy flow in three dimensions," J. Acoust. Soc. Am. 123, 3942.

Rodgers, J., and Nicewander, W. (1988). "Thirteen Ways to Look at the Correlation Coefficient," The American Statician. 42, 59–66.

Roush, D. (2008). 3D Analysis of Azimuthal Dependence of Sound Propagation through Shallow-water Internal Solitary Waves. (Master's thesis, Naval Postgraduate School, 2008).

Zhou, J., Zhang, X., and Rogers, S. (1991). "Resonant interaction of sound with internal solitons in a coastal zone," J. Acoust. Soc. Am. 90, 2042–2054.

THIS PAGE INTENTIONALLY LEFT BLANK

INITIAL DISTRIBUTION LIST

1. Defense Technical Information Center
   Ft. Belvoir, Virginia

2. Dudley Knox Library
   Naval Postgraduate School
   Monterey, California

3. Dr. Ellen Livingston
   Code 321OA
   Arlington, Virginia

4. Professor Kevin B. Smith
   Naval Postgraduate School
   Monterey, California

5. Professor John A. Colosi
   Naval Postgraduate School
   Monterey, California